COMPARISON OF HEMODYNAMIC RESPONSE NON-LINEARITY USING SIMULTANEOUS NEAR INFRARED SPECSTROSCOPY AND MAGNETIC RESONANCE IMAGING MODALITIES

by

RENUKA PARLAPALLI

Presented to the Faculty of the Graduate School of

The University of Texas at Arlington in Partial Fulfillment

of the Requirements

for the Degree of

MASTER OF SCIENCE IN BIOMEDICAL ENGINEERING

THE UNIVERSITY OF TEXAS AT ARLINGTON

August 2008

ACKNOWLEDGEMENTS

First and foremost, I would like to thank Dr. Hanli Liu for giving me an excellent opportunity to pursue my interest in this challenging and cutting edge research project. Her constant support and suggestions throughout the course of my research have been very valuable.

I am sincerely thankful to Dr. Kaundinya Gopinath for his guidance and opinions on the approach of my project. A very special thanks to Dr. Richard Briggs for collaborating with us on this project. I am very grateful to Dr. Georgios Alexandrakis for serving on my committee and providing suggestions to better my thesis.

I would like to immensely thank Mr. Vikrant Sharma for his invaluable technical and moral support; his views have been very useful. I would also like to thank Dr. Fenghua Tian for his comments during the data analysis process. I would like to acknowledge Victoria Vescovo, Umesh Bangalore and Sameer Dhamne for their help during the data acquisition process. I am indeed thankful to all my lab mates for their timely support.

Finally, I am indebted to my family and friends for their encouragement, unwavering support and endless patience.

July 10, 2008

ABSTRACT

COMPARISON OF HEMODYNAMIC RESPONSE NON-LINEARITY USING SIMULTANEOUS NEAR INFRARED SPECSTROSCOPY AND MAGNETIC RESONANCE IMAGING MODALITIES

Renuka Parlapalli, M.S

The University of Texas at Arlington, 2008

Supervising Professor: Hanli Liu

Blood oxygenation level dependent (BOLD) response, which is measured by functional magnetic resonance imaging (fMRI), is known to be a combination of various vascular parameters, among which deoxy-hemoglobin is argued to be a major contributor. Functional near infrared spectroscopy (fNIRS) though limited in its spatial resolution provides a promising tool to study cortical activations, due to its specificity of independent measurement of blood parameters (Oxy, De-oxy and Total Hemoglobin), high temporal resolution and ease of use. To

integrate the best aspects of two imaging modalities, it becomes important to study the close relationship between the two imaging modalities. A finger tapping task with different stimulus durations (2, 4, 8 & 16 sec) with variable inter-stimulation intervals was chosen to compare spatio-temporal properties and non-linearity of BOLD signal with HbO, HbR and HBT signal. This study helped determine what parameters (HbO, HbR and HbT) BOLD correlate to most and how factors like neural adaptation that cause non-linearity can affect the hemodynamic behavior. It investigates the non-linearity in oxy, deoxy and total hemoglobin concentrations as compared to BOLD signal obtained using simultaneous fNIRS and fMRI measurement. Separating non-linearity from hemodynamic response could lead us to a better understanding of neuronal function by modeling neural adaptation. The paper also discusses a method to model the neural adaptation and hemodynamic response.

This information if available could be valuable, especially for the cases where MRI is not so convenient to use (for example, be children with cerebral palsy.

TABLE OF CONTENTS

LIST OF ILLUSTRATIONS

Figure Page

LIST OF TABLES

Table Page

CHAPTER 1

INTRODUCTION

1.1 Principles of Near Infrared Spectroscopy

1.1.1 Diffuse Optical Imaging

Visible light and near-infrared (NIR) light interact with biological tissues predominantly by process of absorption and elastic scattering. There are many physiologically interesting molecules having characteristic absorption spectra at these wavelengths. Particularly, the spectra of oxy-hemoglobin (HBO) and de-oxy hemoglobin (HB) differ markedly, so do the spectra of other chromophores.

Hemoglobin concentrations can act as an indicator of blood volume and oxygenation in the tissue of interest. While most of the physiological information is contained in the absorption coefficient (the number of absorption events occurring per unit length, μa), the scatter coefficient (the number of scattering events occurring per unit length, μs') in tissue is generally considerably larger, hence the signals measured over distances of a few millimeters or larger are dominated by diffuse light.

Different absorption spectra of HBO and HB are regularly exploited in physiological monitoring techniques such as pulse oximetry and near-infrared spectroscopy (NIRS). Diffuse optical imaging (DOI) is a spectroscopic method capable of non-invasively measuring changes in the concentrations of oxy- and deoxy2 hemoglobin, [HBO] and [HB], respectively, by measuring their effect on the optical absorption properties within the tissue [1]. DOI methods use a grid of

interlaced source-detector pairs with overlapping measurement volumes, such that each detector receives light from multiple distinguishable sources. The main aim of this imaging method is to process this information further to produce spatially resolved images. These images may display the specific absorption and scattering properties of the tissue, or physiological parameters such as blood volume and oxygenation, or oxy- & de-oxy- hemoglobin concentrations [2].

Functional optical brain imaging techniques require a faster data acquisition rate for filtering undesired hemoglobin changes arising from various physiological factors. It is also necessary to cover large brain areas; such spatial coverage is not limited to the activation area but extended to the areas that are not involved with the stimulation. This helps in getting contrast between regions of activation and surrounding.

1.1.2 Electromagnetic Spectrum

Light is an electromagnetic wave in the visible region of the electromagnetic spectrum, and it is characterized by its wavelength and frequency. White light is composed of many different wavelengths. Light of different wavelengths is perceived as different colors by the human eye. The visible part of the electromagnetic spectrum (see Figure. 1.1) ranges from ~400 nm (violet/blue) to ~700 nm (red). The near infrared (NIR) light is a type of electromagnetic wave that has a longer wavelength than that of visible light region, it falls between 700 nm – 1000 nm, and it is slightly beyond what the human eyes can see.

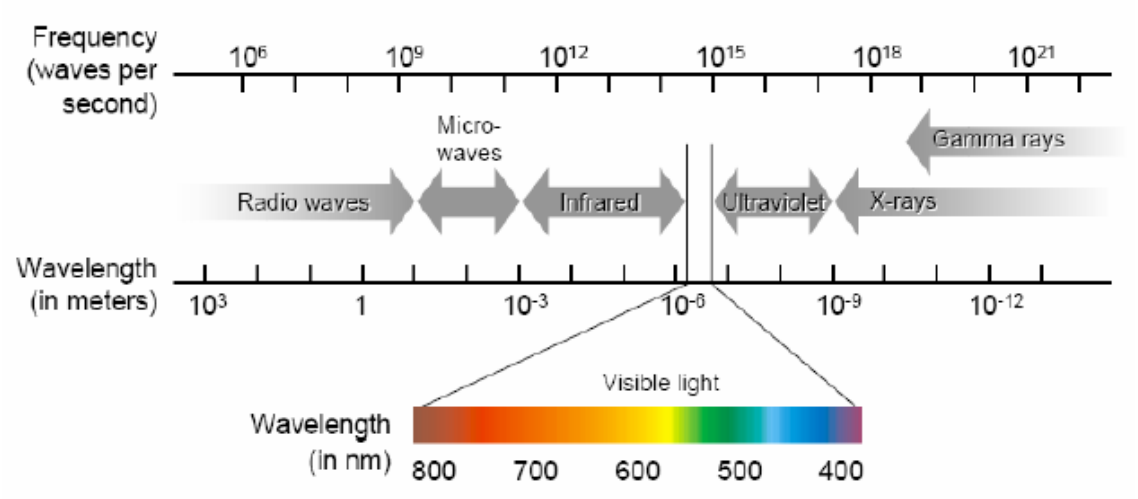

Figure-1.1: Electromagnetic Spectrum [3]

The wavelengths in the NIR region are completely harmless for skin exposures, and no radiation effects are known [3]. The fundamentals of the diffuse optical imaging system utilize the better penetrating near infrared light, rather than visible light, to measure changes in blood hemoglobin concentrations in deep tissue [4].

1.1.3 Optical Window

Light absorption in tissue occurs due to excitation of atoms or molecules to higher energetic states by photons, which are getting destroyed in the process. For a material, the absorption coefficient (μa) varies at different wavelengths, producing so called absorption spectrum for that material. Different molecules or atoms have their own characteristic absorption spectra ("spectroscopic fingerprints"). The spectra of two principal chromophores in diffuse optical imaging (oxy- and deoxy- hemoglobin) areshown in Fig.1.2. DOI operates at wavelengths in the near-infrared range, around 700 to 900 nanometers. This spectral range is

called a “window of transparency” because it allows light to propagate relatively deeply into the tissue before getting absorbed.

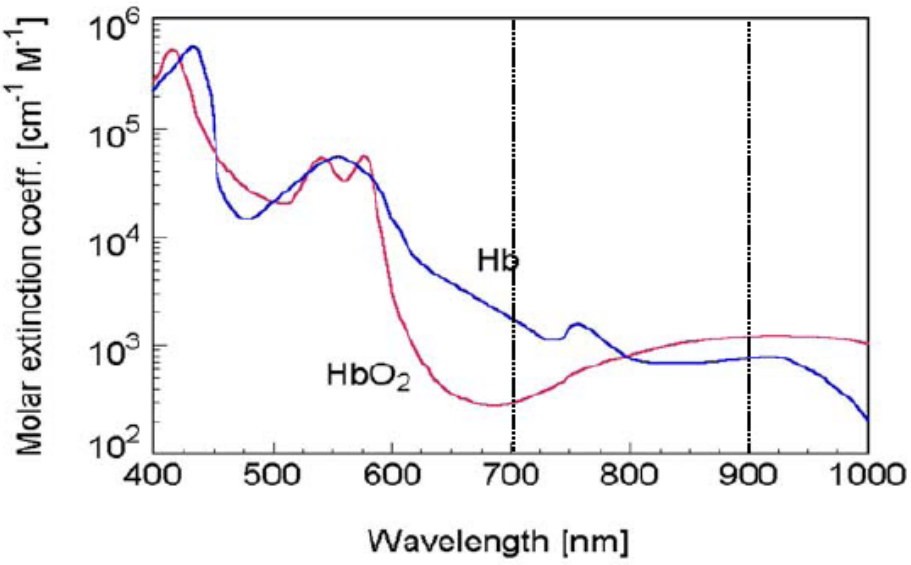

Figure-1.2: Absorption Spectra for oxy and deoxy- hemoglobin [3]

At longer wavelengths the absorption spectrum of water rises steeply, whereas toward lower wavelengths, blood becomes a strong absorber, essentially blocking all light transmission within a few millimeters. Measurements at multiple source wavelengths allow the relative contributions of each component to be calculated independently. Thus DOI can measure changes in [HB], [HBO] and [HBT] simultaneously.

1.1.4 Modified Beer-Lambert Law (MBLL)

A model of light diffusion through tissue is required to quantify changes in concentrations of absorbing species. A traditional approximation to the full photon migration theory is called the modified Beer-Lambert Law (MBLL), which is an empirical description of optical attenuation in a highly scattering medium. Whenever there is a change in the

concentration of an absorbing species, the detected light intensity also changes [5]. As per MBLL, the concentration change is proportional to the logarithm of the detected light intensity during the change divided by the light intensity before the change, as given in eq. (1.1).

$$OD = \log(Io / I) = \epsilon cL \qquad (1.1)$$

where OD is the attenuation measured in optical densities, Io is the light intensity before the change of concentration, I is the light intensity after the change of concentration, c is the concentration of absorbing species, ϵ is the extinction coefficient of absorbing species, and L is the path length through the tissue. This proportionality constant consists of two, simple conceptual pieces: (1) the extinction coefficient of the absorbing species (which can be looked up in the literatures for a particular species) and (2) a measure of the path length the scattered light actually traveled through the tissue (decomposed as the source-detector separation times a quantity called the differential pathlength factor, DPF, i.e. L = d.DPF). The source-detector separation can be easily measured from the probe geometry. The differential pathlength factor is either measured (with a time-domain or frequency domain instrument) or estimated (for a continuous wave measurement).

As already mentioned in the previous section, in order to determine the contribution of multiple chromophores (e.g., oxy- and de-oxy hemoglobin), one must take measurements at one or more wavelengths per chromophore to be resolved. For example, by measuring the change in light intensity at two wavelengths, and using the known extinction coefficients of oxy-hemoglobin ($\varepsilon HbO2$) and de-oxy hemoglobin (εHb) at those wavelengths (from Figure 2), one can then separately determine the concentration changes of oxy-hemoglobin and de-oxy hemoglobin by solving the two equations with two unknowns forΔ[Hb] and Δ [HbO2] [6].

$$\Delta[HbO_2] = \frac{\varepsilon_{Hb}^{\lambda_2}\Delta OD^{\lambda_1} - \varepsilon_{Hb}^{\lambda_1}\Delta OD^{\lambda_2}}{L(\varepsilon_{Hb}^{\lambda_2}\varepsilon_{HbO_2}^{\lambda^1} - \varepsilon_{Hb}^{\lambda_1}\varepsilon_{HbO_2}^{\lambda_2})}$$

$$\Delta[Hb] = \frac{\varepsilon_{HbO_2}^{\lambda_2}\Delta OD^{\lambda_1} - \varepsilon_{HbO_2}^{\lambda_1}\Delta OD^{\lambda_2}}{L(\varepsilon_{Hb}^{\lambda_1}\varepsilon_{HbO_2}^{\lambda_2} - \varepsilon_{Hb}^{\lambda_2}\varepsilon_{HbO_2}^{\lambda_1})}$$

$$\Delta[Hb]_{total} = \Delta[Hb] + \Delta[HbO_2]$$

Where,

OD^{λ} → Optical density at wavelength λ

$\varepsilon HbO2^{\lambda}$ → Extinction coefficient of oxy-hemoglobin at wavelength λ

εHb^{λ} → Extinction coefficient of deoxy-hemoglobin at wavelength λ

1.2 Principles of Magnetic Resonance Imaging

1.2.1 MR Signal Generation

The human body consists of billions of hydrogen nuclei (i.e., protons) found in water molecules that rotate about a natural axis (see Fig. 1.3 (a)). When a person lies in the scanner (see Fig. 1.3 (b)) [7], these nuclei align with the strong main magnetic field. A second electromagnetic field, which oscillates at radiofrequencies and is perpendicular to the main field, is then pulsed to push a proportion of the protons out of alignment with the main field (see Fig. 1.3 (c)).

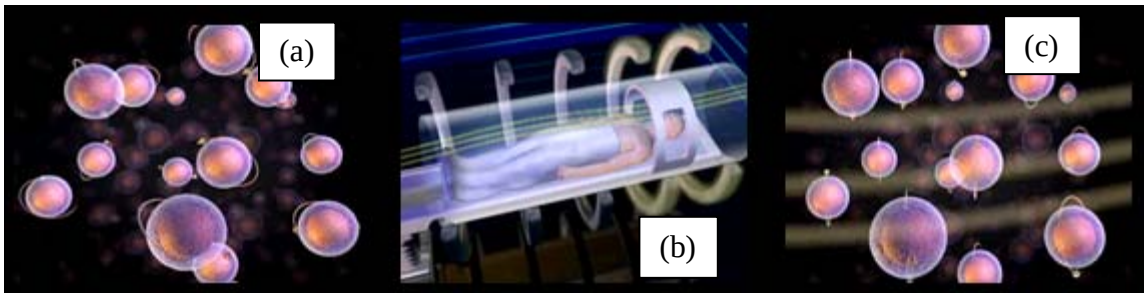

Figure-1.3: (a) Hydrogen nuclei in natural axis [7], (b) Person in scanner with green lines representing magnetic field generated [7], (c) Hydrogen nuclei alignment in presence of magnetic field [7]

1.2.2 MR Image Formation

These protons then drift back into alignment with the main field, emitting a detectable radiofrequency signal as they do so. Since protons in different tissues of the body (e.g., fat vs. muscle) realign at different speeds, the different structures of the body can be revealed. Denser tissues take longer to realign then softer tissues. Hence, the energies emitted by the protons vary. (see Fig. 1.4 (a)).

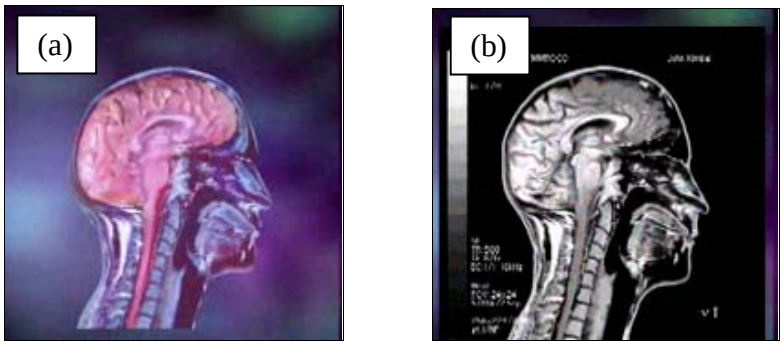

Figure-1.4: (a) Energy spectrum emitted by different tissues [7] (b) MRI Scanner representation of image [7]

MRI Scanners can be used to view different parts of the body in 3 slice orientations/planes – axial, sagittal and coronal. When these slices are viewed in an MRI

Scanner, the denser tissues are represented as black and the softer tissues are represented as white (see Fig. 1.4 (b))

1.3 Brain Physiology

The primary goal of functional imaging is to create images of physiological activity which is correlated with neuronal activity. Information processing or any other kind of activity of neurons increased their metabolic requirements. To meet these requirements, energy must be provided. The vascular system supplies cells with two fuel sources, glucose and oxygen, the latter bound to hemoglobin molecules. So changes in activity of certain region will be accompanied by changes in hemoglobin concentration in that region. These changes will affect the optical density of that region and hence can be detected by an optical brain imager. Blood oxygenation level dependent (BOLD) signal measured by functional magnetic resonance imaging (f-MRI) is known to be due to a combination of various vascular parameters amongst which de-oxy is argued to be a major contributor. Hence, these changes can also be detected in an MRI image

1.3.1 Neurovascular Coupling

Neurovascular coupling helps in understanding the relationship between neuronal activity and the associated hemodynamic changes. A complete understanding of this phenomenon is crucial for interpreting functional imaging data and normal brain function (see Fig. 1.5) [6].

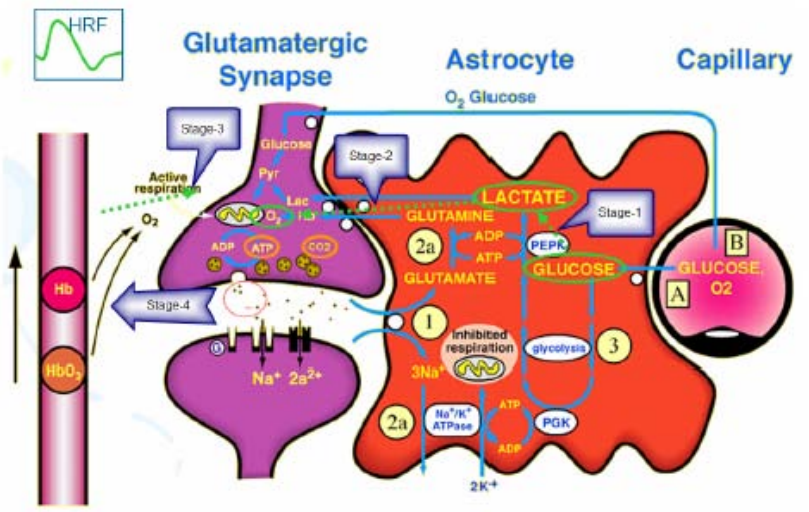

Figure-1.5: Different stages of neurovascular coupling

Neurons have an intimate relationship with astrocytes, smooth muscle, endothelial cells, pericytes, and erythrocytes. Neuronal chemoelectrical activity is speculated to be linked to several metabolic cascades, collectively known as neurovascular coupling. Neurovascular coupling includes the following stages:

(1) Glucose is metabolized to lactate in astrocytes (anaerobic glycolysis),

(2) The lactate is then shuttled to neurons and metabolized with oxygen to form carbon dioxide and ATP.

(3) Arteries deliver oxy-hemoglobin to neurons, and oxygen is then released in the presence of carbon dioxide, thus converting oxy-hemoglobin into deoxy-hemoglobin.

(4) Nitric oxide or neurotransmitters, such as acetylcholine released by active neurons, cause relaxation of smooth muscle in arterioles, thus increasing blood flow and volume.

Functional brain imaging techniques, such as EEG, PET, fMRI, or DOI, detect the changes in signals during one or more of these events during neurovascular coupling.

1.3.2 Motor Cortex

The brain is divided into cerebrum, cerebellum and medulla oblongata. The motor cortex is found in the regions of the cerebral cortex that is involved in planning, control and execution of voluntary activities. The motor cortex is divided into five main areas: Primary Motor Cortex (M1), Secondary Motor Cortex, Pre-motor Cortex, Posterior Parietal Cortex, Supplementary Motor area (see Fig. 1.6(a)).

The primary motor cortex is responsible for generating neural impulses controlling movement. The M1 region connects the brain with the lower motor neurons via the spinal cord. This helps them to know which particular muscle needs to contract. The M1 region works in coordination with the pre-motor areas to plan the execution of movements [8].

The lateral area of the primary cortex is divided from top to bottom based on different parts of the body movement. The area occupied on the motor cortex depends on the complexity of movement carried out by a particular body part (see Fig. 1.6(b)).

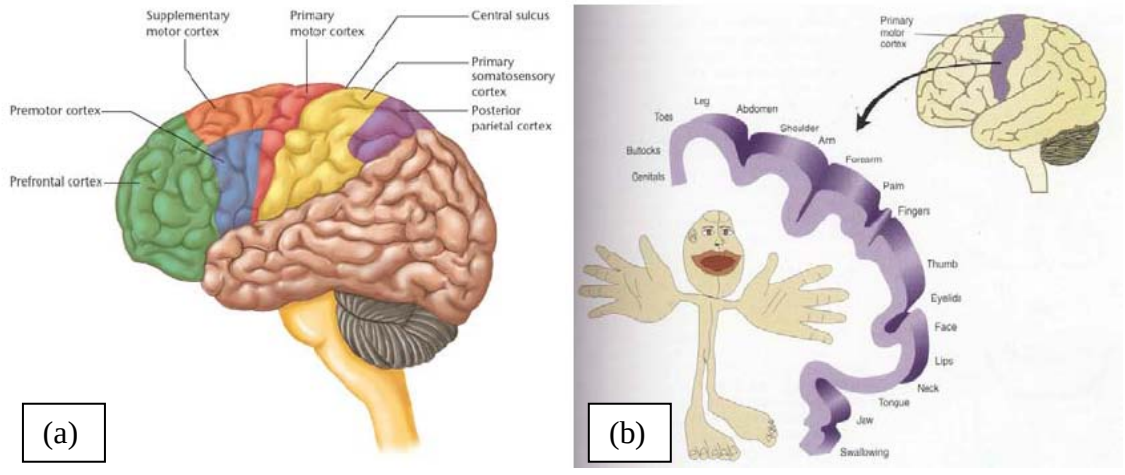

Figure-1.6: (a) Brain Anatomy (b) Homunculus diagram of the motor cortex

This arrangement is known as Homunculus ("little person"). It shows that there are disproportionate amount of cortical areas devoted to movements of the fingers and muscles used for speech [8]. Hence it is also true that movements of limbs, hands, fingers etc. accordingly activate the associated areas of the motor cortex.

1.3.3 Breath hold physiology

The respiratory system is crucial in maintaining homeostatic levels of blood gases. Cells and tissues in our bodies are very sensitive to minor changes in levels of oxygen and carbon dioxide in our blood. Throughout our circulatory system exist numerous sensors that constantly monitor O2, CO2, and pH levels to insure that our tissues are getting enough oxygen to maintain our metabolic pathways.

As one holds breath, the brain cells see an increase in partial pressure of carbon dioxide (pCO2) and see a need for oxygen in the blood stream. Due to vasomotor reactivity, there is a rise in CBF (cerebral blood flow), and this flow increase will enrich the oxy-hemoglobin concentration in the overall blood concentration. On the other hand, the depletion of oxygen stores in the body during breath holding will increase the overall concentration of deoxy-hemoglobin in the blood [9].

CHAPTER 2

METHODS

2.1 Subjects

In this study, we enrolled 5 healthy, right handed subjects (4 males and 1 female). The subjects were 20-40 years old. This University of Texas, Arlington Institution Review Board approved the study, and all subjects gave written informed consent. For the BOLD-NIRS comparisons, all 5 subjects enrolled were scanned. Two subjects failed to show any significant activation (extremely poor signal to noise ratio) in NIRS and hence were excluded from the study as the comparison in both modalities was not possible for these cases. The remaining 3 subjects were included in the data analysis.

2.2 Protocol

Prior to the placement in the bore of the MRI Scanner, subjects were briefed on the finger tapping task. A total of four finger tapping protocols of durations 2, 4, 8 and 16 seconds were used with variable inter-stimulation intervals (ISI) and were repeated for 16, 16, 12 and 9 blocks respectively. A variable ISI protocol is typically chosen to minimize the subject's anticipation of the next block within a protocol run and to provide uniform temporal coverage necessary for

deconvolution. The same set of protocols was used to study the spatio-temporal properties and the nonlinear hemodynamic response of oxy, de-oxy and total hemoglobin in comparison to the BOLD signal. The details of the ISI and the number of blocks of each protocol are indicated in Table 1.

Table 1: Variable ISI and number of blocks for each protocol

2 sec protocol ISI	4 sec protocol ISI	8 sec protocol ISI	16 sec protocol ISI
12 s	12 s	16 s	22 s
14 s	14 s	16 s	18 s
12 s	12 s	14 s	22 s
10 s	14 s	14 s	22 s
10 s	12 s	14 s	20 s
10 s	12 s	18 s	20 s
10 s	10 s	16 s	18 s
14 s	10 s	18 s	18 s
12 s	14 s	18 s	20 s
12 s	14 s	18 s	
14 s	14 s	16 s	
14 s	10 s	14 s	
14 s	10 s		
12 s	10 s		
10 s	12 s		
10 s	10 s		
16 BLOCKS	16 BLOCKS	12 BLOCKS	9 BLOCKS

At the beginning of each protocol, the subject was asked to relax for 10 seconds during which baseline was recorded. An additional 10 seconds of relaxation at the end of each protocol was provided (Figure 2.1). The visual instructions of TAP and RELAX for this protocol were provided by the e-prime software. During the taping phase, the subjects were asked to sequentially tap fingers of their right hand in a thumb opposition mechanism at a self paced rate (~2-3) Hz.

A simple breath hold (BH) protocol of three runs was also adopted to see how similar the activation maps were for a breath hold protocol over a finger taping protocol in both the modalities. Each BH run had three blocks. At the beginning of each run, the subject was asked to relax for 10 seconds, during which baseline was recorded. The subject was then instructed to hold his/her breath for 20 seconds and then relax (or re breathe) for 40 seconds. Each subject performed the BH protocols after the finger tapping protocols.

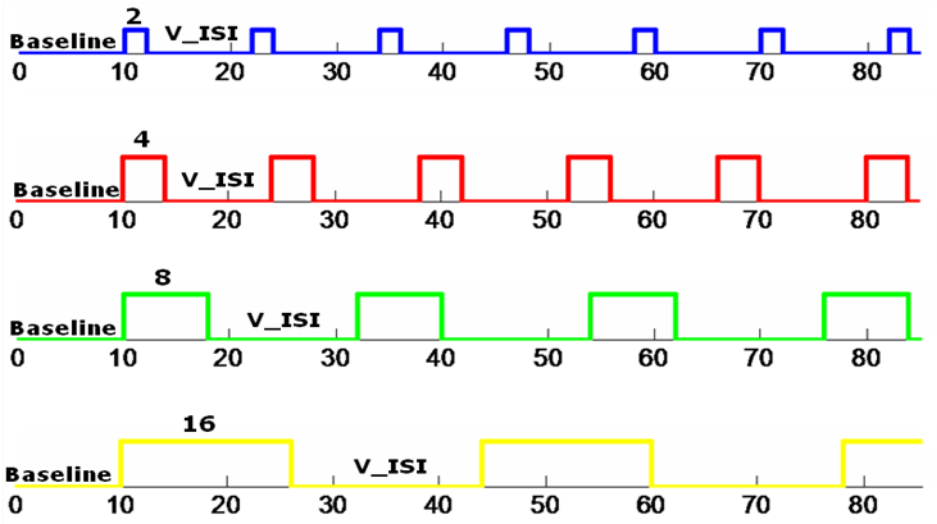

Figure-2.1: Timing Diagram of the finger tapping protocol

2.3 Probe Design

For this study, 8 laser sources (at 690 nm, 830 nm) and 8 detectors were used with a 3-cm, source-detector separations as shown in figure 2.2. The probe design consisted of alternating rows of four sources and four detectors each. The left cerebral hemisphere is known to control the right (contralateral) side of the body and vice-versa. Hence, only the left portion of the probe holder was used for this study as indicated in the figure 2.2. In order to ensure that the probe holder was placed over the motor cortex, manual method was used to localize the motor cortex.

A vertex was obtained at the intersection of two Velcro straps; one from nescient to anion and the other from ear to ear. The probe is placed in such a way that vertex lied equidistant from the middle to rows.

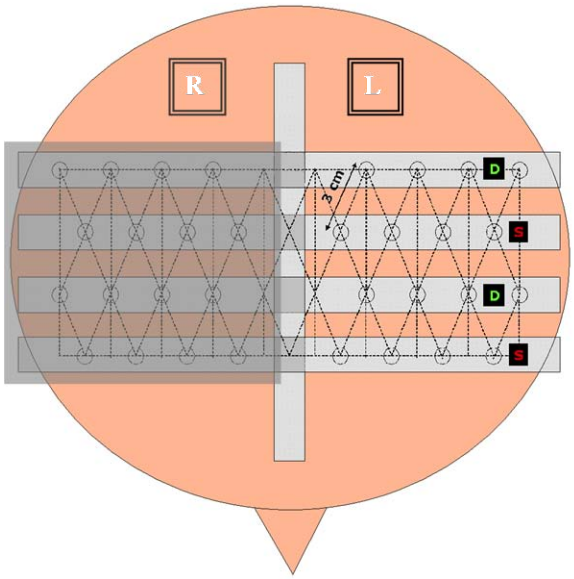

Figure-2.2: Probe design and placement in axial view; triangle represents the nose; R – right cerebral hemisphere; L – left cerebral hemisphere

To visualize the optical probe in the MRI Scans, vitamin E capsules were placed at each optode on the probe holder [10]. Figure 2.3 indicates the position of these vitamin E capsules in an image obtained after 3D Volume Rendering using a software called Osirix.

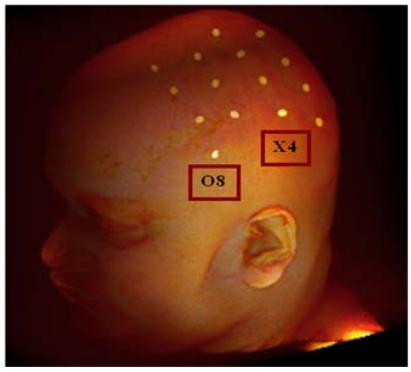

Figure 2.3: Visualization of Vitamin E capsules in an image after 3D Volume Rendering

2.4 Optical Imaging System

2.4.1 Continuous-Wave (CW) Systems

These systems emit light continuously at constant amplitude, or modulated at low frequencies (of the order of few tens of kilohertz) or use time multiplexed illumination. CW systems measure only the amplitude decay of the incident light. The main advantages of this system include higher sampling rate, less weight, simplicity and relatively cheap cost. The disadvantages of such a system include lower penetration depth and the inability to separate absorption and scattering.

2.4.2 CW5 Imager

The CW5 imager is manufactured by TechEn Inc., Milford, MA. It is designed to perform multi-wavelength, continuous wave, near infrared, diffuse optical tomographic measurements at very high sampling rates (Fig. 2.1). CW5 system uses frequency-division multiplexed laser sources.

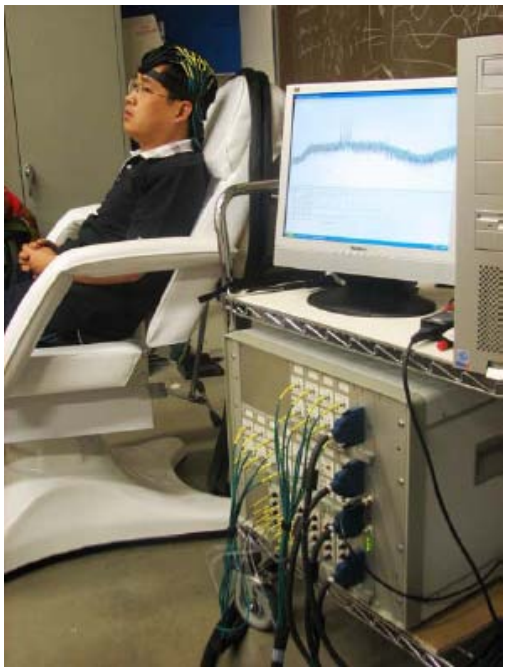

Figure-2.4: CW5 System

The lasers are at two source wavelengths, 690 nm and 830 nm, and split evenly between 24 sources (i.e.12 lasers at each wavelength). The odd numbered lasers function at 690 nm and the even numbered ones at 830 nm. The measured power at the output of 690 nm sources is adjusted to emit near 9 mW and the 830 nm sources near 5 mW power. Lasers are square-wave modulated at a frequency band ranging from 6.4 kHz to 11 kHz, with an interval of 200 Hz between adjacent frequencies. "Continuous parallel operation of all the sources and detectors allows for rapid data collection." [11]

Our CW5 instrument has 24 transmitter channels (lasers sources) and 24 receiver channels (detectors). The unit houses 21 cards: 6 transmitter cards with the four lasers each, 12 receiver cards with two detectors each, one control card with 3 connectors to National Instrument data acquisition cards, and one clock buffer card. Figure-2.5 above shows the locations of the twenty-one cards looking at the front panel of the instrument [12].

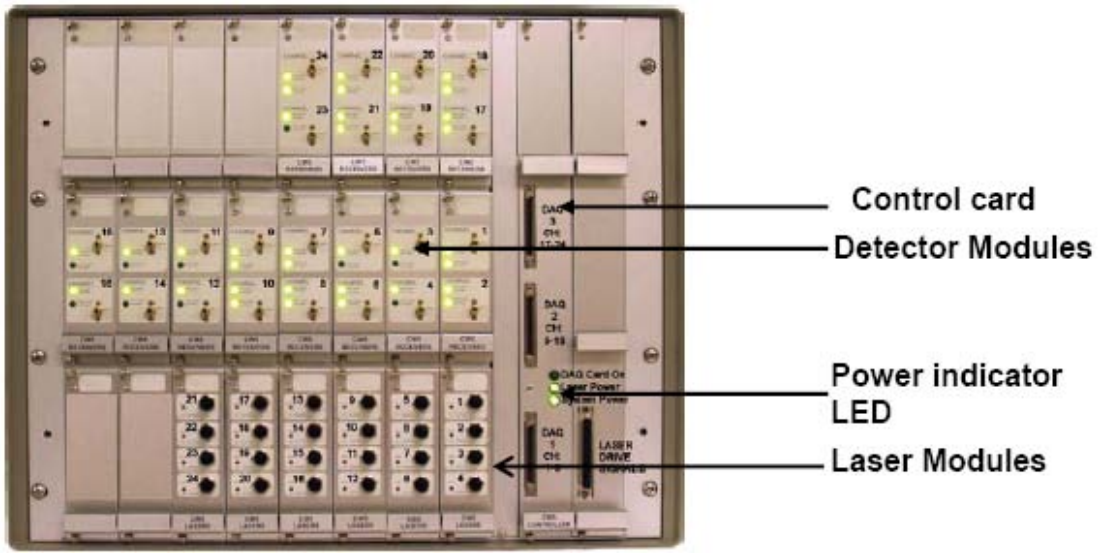

Figure-2.5: Front Panel of CW5 System

Our CW5 instrument has 24 transmitter channels (lasers sources) and 24 receiver channels (detectors). The unit houses 21 cards: 6 transmitter cards with the four lasers each, 12 receiver cards with two detectors each, one control card with 3 connectors to National Instrument data acquisition cards, and one clock buffer card. Figure-2.5 above shows the locations of the twenty-one cards looking at the front panel of the instrument [12].

Figure-2.6 shows laser source transmitter card and receiver card for the system. Each laser source card has four sources, 2 of each wavelength. The system has 6 such cards arranged in parallel on the front panel, giving 12 sources of each wavelength.

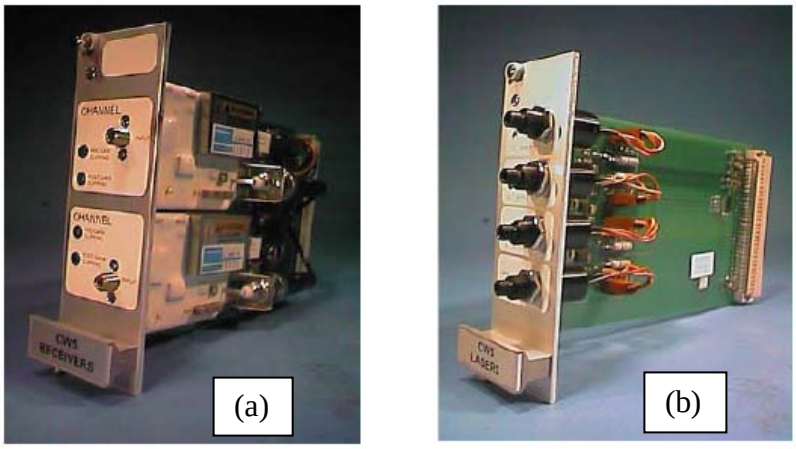

Figure-2.6: (a) Transmitter Card (b) Receiver Card [12]

Each receiver card has two APD detectors, 12 such cards are present on the system making the total number of detectors to 24. The 24 receiver channels generate a set of 24 single ended analog signals. The controller (shown in figure-2.5) buffers and converts these 24 single ended signals to 24 differential pairs and drives them out the analog signal connector [12].

2.4.3 Optical Data Processing Environment

All the data that is acquired using the CW-5 imaging system discussed above is processed using a software called HoMER (Hemodynamic Evoked Response).

HomER is a graphical user interface developed to analyze the functional Near- Infrared Spectroscopy (NIRS) data. It has tools for filtering, data averaging, linear regression, and 2D image reconstruction. "HomER is designed to work with NIRS data from most source and experimental set-ups, allowing the user full control of the measurement configuration and probe properties" [14]

HomER can be divided in to 4 sub sections: Section-1: Signal Processing, Section-2: Response Processing, Section-3: Image Reconstruction, Section-4: Region of Interest Analysis.

Section-1: Signal processing

This section of HomER incorporates windows displaying raw data and probe geometry. It contains tools for filtering time-courses with band-pass filters and principal component analysis (Fig. 2.4). PCA helps in removal of systemic fluctuation and artifact. [14]

Section-2: Response Processing

This section of HomER is dedicated for analyzing functional hemodynamic responses. In addition to multiple condition experimental designs, this also supports block-designed and event-related paradigms. The hemodynamic response curves are displayed as per their respective optode location, which helps in localization of activity. Responses can be analyzed for entire experimental run or can be averaged over blocks of time interval.

Section-3: Image Reconstruction

HomER offers various options for basic image reconstruction including backprojection and other regularized inversion techniques. This section is capable of reconstructing both optical density and hemoglobin concentration images. The response time for reconstruction can be varied with the help of Slide bar, allowing better control over image reconstruction. The imaging parameter control menu provides the options for varying the absorption and scattering coefficients, the voxel sizes and reconstruction depths.

Section-4: Region of Interest Analysis

Section-4 of HomER has the capability of performing Region-of-Interest (ROI) analysis. ROI averages can be calculated for individual subjects or group of subjects and across multiple sessions. The regions of interest can be defined by source-detector channel or within the

reconstructed image. It calculates the Hemodynamic Response Function (HRF) for the selected region. Comparison between response functions of various subjects can be done in this section.

2.5 Magnetic Resonance Imaging System

A MRI Scanner with magnetic field of 3T manufactured by Siemens Inc. was used for this study

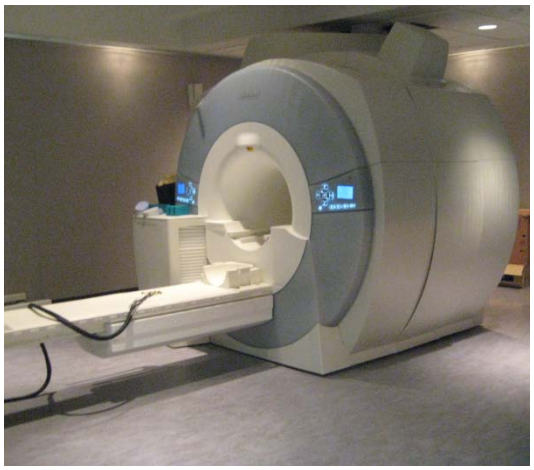

Figure 2.7: 3T Siemens MRI Scanner

2.5.1 Data Acquisition Parameters

A whole- brain high resolution fMRI data was acquired with an echo-planar imaging sequence. The TR, TE and flip angle used for the study are 2000 msec, 24msec and 90° respectively. A field of view (FOV) of 220 mm X 220 mm was chosen. The slice thickness for acquisition was set to 3.2 mm. Forty such slices were acquired at 3.0 mm X 3.0 mm resolution to ensure that the entire brain was covered. The scan time fed in varied from protocol to protocol.

For anatomic reference a T1-weighted 1 mm x 1mm x1mm whole brain MPRAGE sequence. The TR, TE, TI and flip angle were set to 2250 ms, 2.8 ms, 900 ms and 9º respectively. Images were acquired at a resolution of 0.9 mm X 0.9mm X 1.1 mm. The FOV was set to be 240 mm (read) X 240(phase) mm X 160 mm (slice). A Time-Of-Flight MRA sequence with same slice locations as the fMRI runs was acquired for angiographic reference. The TR, TE and flip angle used were 26 ms, 6.9 ms and 50º. These images were acquired at a resolution of 0.9 mm X 0.9mm X 3.2 mm.

2.5.2 MRI Data Processing Environment

Standardization is an important aspect for producing high quality fMRI. Once the fMRI examination is complete an image data is collected, post processing is required to extract the functional data. The processing of functional data is quite complex though sophisticated especially when event related paradigms are used. Processing algorithms and statistical analysis are used to correlate the presentation of stimuli with the collection of brain images. In many cases, these algorithms have been incorporated into existing computer applications such as Analysis of Functional Neuro Images (AFNI), SPM and Brain Voyager (BV). Activity is frequently represented as the change in MR signal observed during performance of a particular activity relative to a baseline condition of rest. Statistical maps can be then transformed, rendered and superimposed onto anatomical images for visualization and interpretation [15]

.

AFNI is a set of C programs for processing, analyzing, and displaying FMRI data. One of AFNI's particular strength is that it is a powerful tool to display functional data.

2.6 E-PRIME Software

E-prime software consists of a suite of applications which can comprehensively fulfill research needs. It is capable of generating experiments, collecting data with milliseconds precision through data handling and processing. It also provides a user-friendly environment and the flexibility of creating simple and complex experiments. In my study e-prime studio package was mainly used to provide visual display of the protocol to the subject [16].

2.7 BIOPAC Physiological Monitoring System

BIOPAC is a readily available data acquisition system. In my study BIOPAC was primarily used for monitoring the respiration and the heart rate of the subject during the experiment.

2.8 Experimental Setup

The CW-5 imager was placed in the MRI console room and the optical fibers (sources and detectors) were sent through the wave guide into the MRI Scanner Room. All 16 (8 sources and 8 fibers) 30 ft fibers were wrapped in a sleeve and passed as one long bundle into the scanner room (Figure 2.8). The exposed source fibers (without the casing) and the detector fibers (with the casing) are MRI compatible.

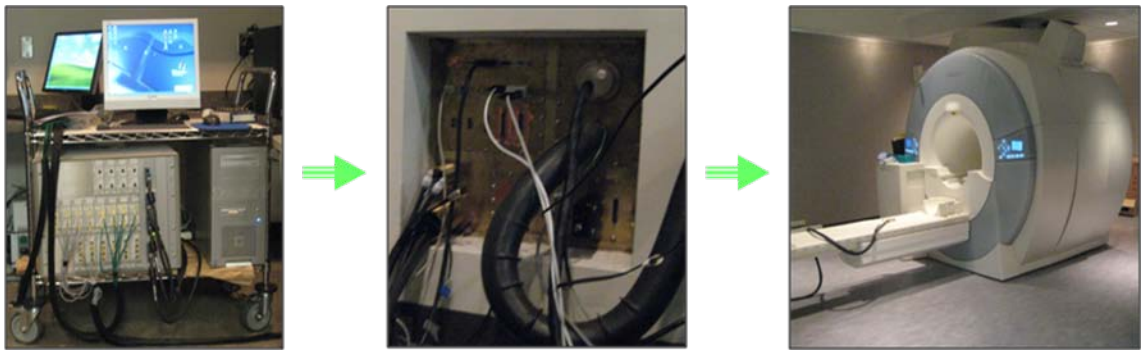

Figure 2.8: Experimental Setup I

Once, the subject signs the consent form, the probe is placed on the subject as discussed in the previous section. It was ensured that every single probe made good contact with the scalp through visual inspection. Multiple Velcro straps and an elastic head wrap are used to hold the probe and vitamin E capsules in place to ensure that they do not displace when the subject lies down in the magnet (Figure 2.9). A respiration belt is placed around the subject's chest and a pulse oximeter on the subject's left hand for physiological monitoring.

Figure 2.9: Experimental Setup II

After the subjects are put into the bore of the MRI Scanner, the gains for the CW-5 imager were checked using an automatic gain control provision. The subjects were then instructed to watch a visual display from a projector, which was placed in front of the scanner room onto a screen in the bore of the magnet and was visible from a mirror mounted on the top

of the MR head-coil above the subject's eyes. On the display the main instructions shown where the text 'TAP' and '+'. For the duration of the 'TAP' visual cue, subjects were asked to their thumb and their fingers on the right hand at a self paced rate (approximately 2-3 Hz). After 2s, when the visual cue changed to '+', the subjects were instructed to stop tapping and keep their hand relaxed. Aside from the finger-tapping subjects were instructed to remain motionless for the duration of the scanning session. The subject was given headphones to receive instructions from the MR personnel in the console room (Figure 2.10) and a squeeze ball to report any kind of emergency situation.

The console room had the CW-5 imager, the computer with the E-prime software that was connected to the projector in the scanner room, the physiological monitoring system and the MRI data acquisition system (Siemens). After shimming of the magnetic coils, a T1-weighted MPRAGE image sequence was run for anatomic reference. To ensure that the data collection in all the systems started at the same time the MRI data acquisition system, the physiological monitoring system and the E-prime software were triggered automatically and the CW-5 imager was triggered on a manual count. An echo planar imaging (EPI) sequence was run for each of the finger tapping protocols in the order of 2 s, 16 s, 4 s and 8 s experimental paradigms. After the finger tapping protocols, three runs of the BH protocol were run. During the entire protocol, the subject was told what protocol was next by the MR personnel from the console room.

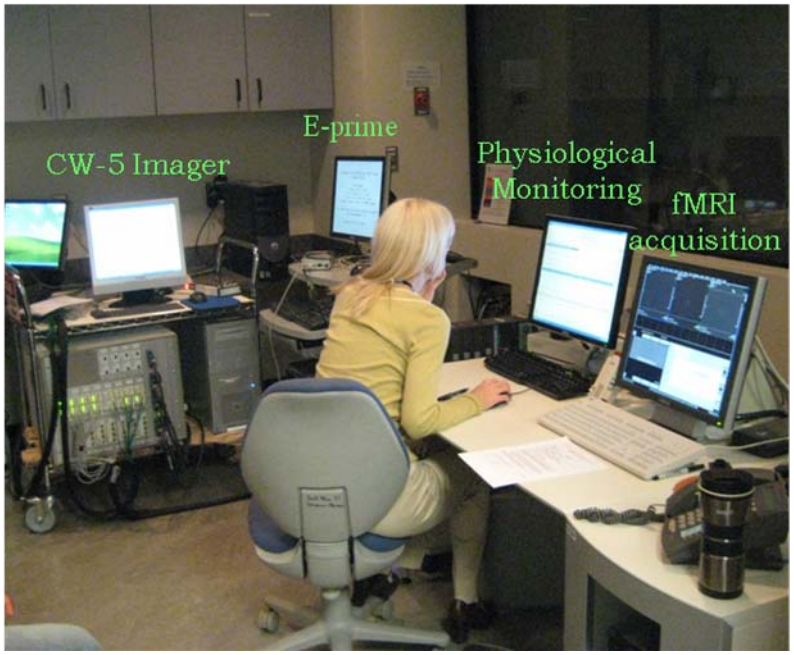

Figure 2.10: Console Room

2.9 Compatibility Issues

The source and detector fibers which are the components of the optical system which enter the bore of the magnet are meant to be MRI compatible. Hence a simultaneous study with the two modalities is expected not to show any artifacts. Surprisingly, a huge artifact was observed in the encircled regions of the MRI Scans (Figure 2.11) right below the location of the optical probe.

Figure 2.11: Artifact seen due to optical probe on the subject

To isolate the problem a phantom test was performed to check what component of the optical probe setup (sources, detectors, Velcro straps, probe holder, etc) was contributing to the artifact. A spherical phantom with a spout was used for the phantom test to represent closest approximation to the human head. The phantom tests clearly indicated that the source fibers (Figure 2.12 (a)), or to be more specific the casing of the source fibers contributed to the significant artifact seen in the figure above. Due to the fragile nature of the fibers, about 60 cm of the casing of the source fibers was stripped off (mainly the portion of the source fibers that went into the bore of the magnet during the experiment) and the phantom test was repeated. The exposed source fibers showed no artifact at all (Figure 2.12 (b)). Therefore, the exposed source fibers were used for the entire study to avoid the artifacts.

(a) 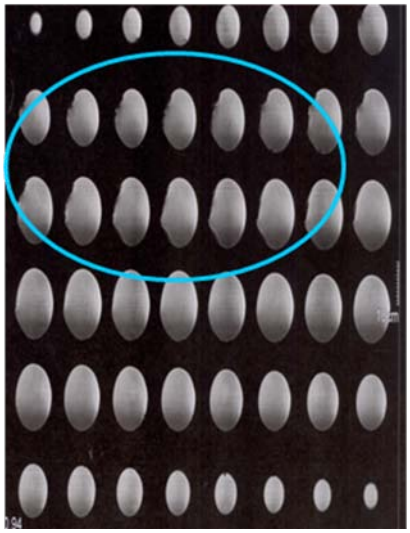 (b) 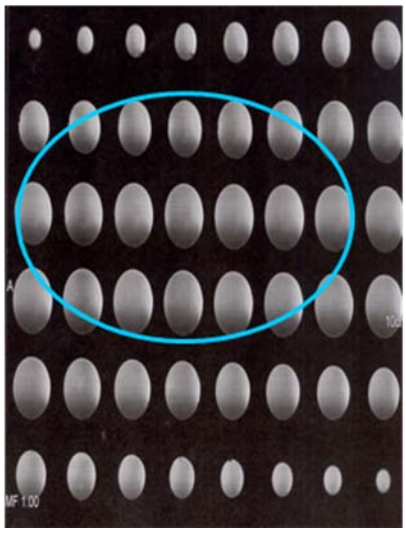

Figure 2.12: (a) Source fibers with casing on spherical phantom (b) Exposed source fibers on spherical phantom

2.10 Nonlinearity model

Any linear system must follow two basic principles

(a) Scaling: It states that the magnitude of the system output must be proportional to the system input [17].

(b) Superposition: It states that the total response to a set of inputs is equivalent to the summation of the independent responses to the input [17].

Early experiments [18] pointed to a linear relationship between stimulus parameters, such as duration and the hemodynamic response. Others [19] in literature have shown that a linear system analysis can be used to model the BOLD response. However, in recent times another possibility that has been examined is that the hemodynamic response to a given stimulus may be affected by what other stimuli are presented to it. If two stimuli are presented very close together, the combined response might be less than the sum of the two individual responses. Reduction in

hemodynamic amplitude as a function of the interstimulus interval are known as refractory effects. If refractory effects are present, then a linear model will overestimate the hemodynamic response to closely spaced stimuli, potentially reducing the effectiveness of experimental analysis/ It is critical, therefore, to consider the evidence for and against the linearity of the fMRI hemodynamic response.

The exact reason for non-linearity in hemodynamic response is unknown. Since a cascade of physiological processes occurs after stimulus presentation, it is likely that multiple factors between the stimulus and the measured response contribute to nonlinearity. Literature indicates that perhaps the non-linearity of BOLD response is caused by a combination of factors such as neural adaptation, blood flow, and oxygen extraction. This study is based on the hypothesis that non-linearity in HbO, HbR and HbT may be due to neural adaptation. Hence, the nonlinearity of the hemodynamic response in both modalities was modeled using a neural adaptation function.

CHAPTER 3

DATA ANALYSIS

This data analysis was broadly done in four parts (1) A spatio-temporal comparison of BOLD responses with optical signals in terms of HbO, HbR and HbT was performed (2) we analyzed the optical signals so as to check for non-linearity in HbO, HbR and HbT and compared it with the non-linearity in the BOLD signal (3) the data was fitted and the fitted parameters were compared with the existing BOLD parameters. fNIRS data was acquired using CW5 (TechEn, Inc.), which is a continuous wave near-infrared brain imager and (4)

3.1 NIRS Data Analysis

Preliminary processing of the NIRS data was done using HoMER. The .cw5 files acquired using HoMER are converted into .nirs format for compatibility with HoMER

1. Filtering: Raw change in concentration of HbO, HbR and HbT was filtered with a low pass filter (LPF) of 0.4-0.5 Hz to remove any kind of physiological noise and a high pass filter (HPF) of 0.01-0.02 Hz was used to remove any baseline drift in the raw data. The

2. HPF was not used for the breath hold data, as this would result in removing the signal due to the breath protocol itself.
3. Averaging: Block averaging was used to maximize the signal to noise ratio. The 2 sec, 4 sec, 8 sec and 16 sec paradigms were averaged over their multiple blocks respectively. For each paradigm the shortest ISI was considered for the block. For example, for the 2 second protocol, an ISI of 10 sec was taken for each block making the block size a total of 12 seconds.
4. Imaging: HoMER provides an activation map with the probe configuration (sources and detectors) thereby showing the highest channel of activation or the area of activation

The pre-processed data was exported to MATLAB for further detailed processing.

3.2_MRI Data Analysis

All the MRI data was pre-processed using AFNI. Pre-processing is an important step in functional image analysis. It is mainly done to remove any variability in data that is not due to the experimental task. There is no standard pipeline for processing fMRI data. The method used may depend on the data design and the data acquisition parameters. The images obtained from the MRI Scanner in this case were pre-processed in a series of steps [15]. These steps are discussed briefly below

1. File conversion *(to3d)*: This command is used to create AFNI datasets. The images obtained from the MRI Scanner are of the .DICOM format. The to3d command converts the .DICOM files into .BRIK and .HEAD files so that the files can be read and analyzed using AFNI.

2. Mask Generation *(3dAutomask)*: This command masks out the non-brain parts in the image
3. Detecting outliers *(3dToutcount)*: This command detects outliers in a sequence of images and checks for image quality. Once the outliers are detected, the corresponding points can be censored.
4. Volume registration *(3dvolreg)*: Functional MRI data consists of multiple brain volumes acquired over time. There is often a possibility of head motion (small of large) during the scan time. For fMRI data to be meaningful, it is necessary to ensure that all the data volumes are properly aligned and motion artifacts are corrected for. AFNI uses 3dvolreg to do volume registration. One of these position-matched functional volumes is chosen as the "base" volume (usually the one closest to the anatomical scan), and all other functional volumes are registered to it. Registration is done at the image level, for example, first image from all the volumes are registered to first image from the base volume.
5. Piecewise linear detrending *(3dTcat)*: Piecewise linear detrending is done using 3dTcat command. The purpose of detrending is to remove any slow drifts in the data, which could be due to physiological or instrument noise.
6. Smoothening *(3dmerge)*: This command if used for spatial smoothening.
7. Ideal Response *(Waver and 1dplot)*: After the data has been pre-processed, our aim is to localize the area of activation on the 3Dvolumetric data. For our block design, we use linear regression analysis with a single regressor. This is done in multiple steps. First a regressor that models the hemodynamic response during the task periods is

generated. A '.txt' stimulus file that contains a single column of 0's (indicating rest) and 1's (indicating stimulus) is created that represents tasks verses rest respectively. The number of elements in the file should be equal to the number of TR's (time of repetition). For instance, in the 16 seconds of stimulus should be represented by 8 1's in the stimulus file.

The stim file obtained consists of a train of square pulses at the stimulus intervals. But, a typical hemodynamic response has a different behavior as compared to a square pulse. The hemodynamic response function (HRF) is convolved with the stimulus train to obtain a lagged regressor which is a better representation of the hemodynamic response. This is called the ideal response.

The ideal response is generated using the Waver function in AFNI generated the ideal response using Waver function in AFNI. Waver takes the input stim file, and places a standard hemodynamic response at the beginning of every TR containing a 1. The parameters (delay, rise time etc.) of the HRF that waver uses can be modified using the option – GAM.

8. Regression Analysis *(3dDeconvolve)*: Once the ideal response is obtained, linear regression analysis is done for each and every voxel time series in the functional data. This is achieved using 3dDeconvolve function in AFNI which calculates the deconvolution of a measurement 3d+time dataset with a specified input stimulus time series. Second order polynomial fit was done using the polort 2 option. The number of the input regressors (i.e.1), the file and name of the input regressors are important parameters that are specified using this function. The options –rout and –fout are used

to specify what is required in the output dataset. Output image consists of an AFNI 'bucket' type dataset containing the least squares estimates of the linear regression coefficients, f-statistics for significance of the individual input stimuli

9. Overlay: In order to view activation in specific voxels a set of parameters have to be set in the AFNI window. The Olay and the Thr tab are used to specify the Regression Coefficients and the f-statistics of the regressor respectively. The intensity color bar is set to 2. The value chosen on the threshold slider is determined empirically. This value is chosen such that activation is obtained only in the region of interest. Once the parameters are set, the activation map is superimposed on the anatomical image to view the exact areas of activation. The underlay image is changed to the anatomical image using the switch underlay command. The overlay image is set to the functional image (e.g. 16 seconds finger tapping functional image) using the Switch Overlay command. The Overlay image can be viewed by checking the See Overlay Tab. These GUI is indicated in Figure 3.1. The overlay step is done for each of the protocols; using the respective functional image as the overlay image with the anatomical image as the underlay image.

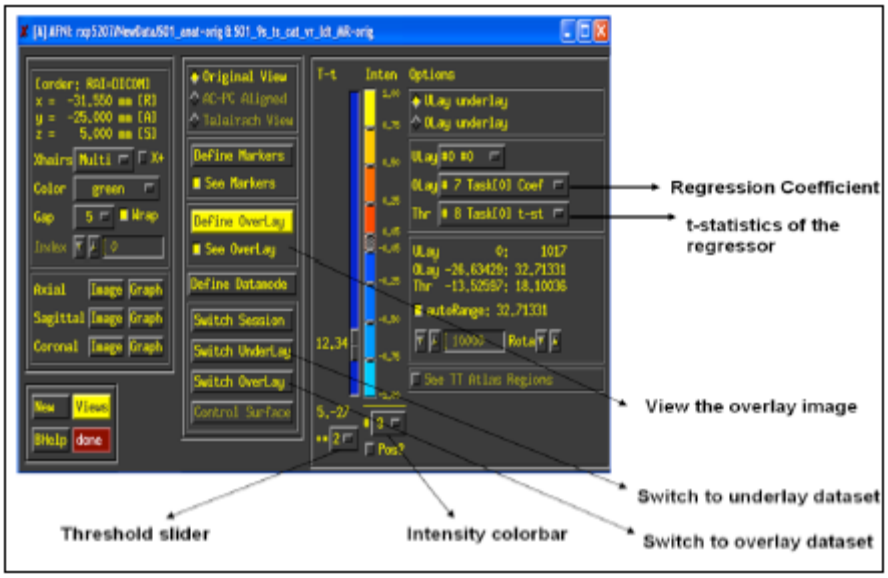

Figure 3.1: AFNI Control Panel

3.2.1 MRI Block Averaging:

All the protocols have been performed in task-block designs in which the subject performs a task successively with no task periods. This is done in order to enhance the statistical power of standard analysis techniques based on correlation or unvariate statistical tests [20]. By averaging over a number of task-block cycles, small consistently task-related (CTR) differences in hemodynamic activation can be detected. Isolated stimulus paradigms avoid overlapping hemodynamic responses produced by more rapid stimulus presentation rates, but interpretation of the responses still involves averaging responses over many different stimulus presentations [21]. The averaging was performed on the 2 seconds, 4 seconds, 8 seconds and 16 seconds protocol data for their respective blocks. Averaging in AFNI can broadly be divided into 2 categories which are discussed below:

1. Single Trial Averaging *(3dcalc)*: The averaging was done using function 3dcalc and by providing the starting and ending TR's for each block of the time series data. This

is done in order to get the hemodynamic response of the stimulus. For each of the protocol's averaged data the x, y, and z axis parameters were chosen such that the center voxel of each region of interest showed maximum activation. This was done by trial and error method.

2. Region of Interest (ROI) averaging *(AFNI Plug in)*: ROI aims at segregating the activated blobs in an image. In my study first the primary motor cortex and pre-central gyrus were located approximately in the axial view (Figure 3.2 (a)). Based on this, at every crosswire position of the region located, a ROI was drawn in the sagittal view (Figure 3.2(b)). All the voxels that lied within the ROI of interest above a certain threshold value were averaged out and considered to be part of the final region of interest.

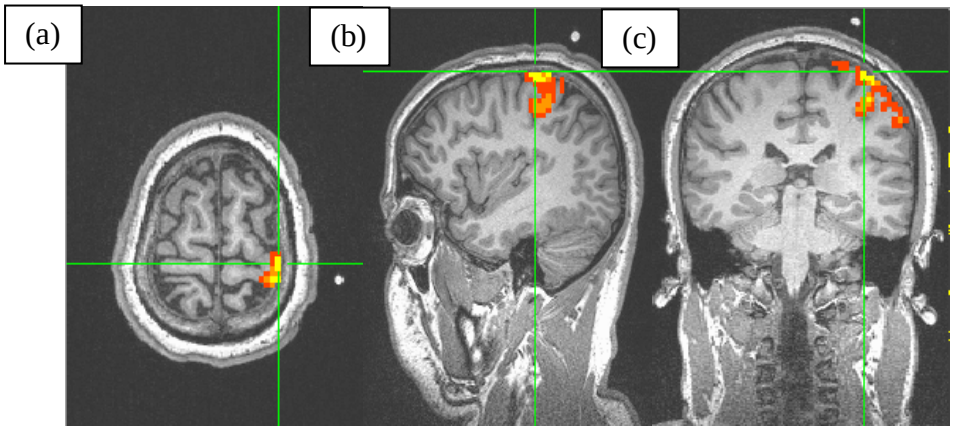

Figure 3.2: (a) Axial View (b) Sagittal View (c) Coronal View for ROI averaging analysis

All the files processed here were written in a one dimensional array format (1D format) and exported to MATLAB for further detailed processing.

CHAPTER 4

RESULTS

4.1 Spatio-temporal response comparison.

4.1.1 Spatial Response Correlation

The first part of the study was aimed at spatially correlating the block averaged hemodynamic response properties of the two modalities. In NIRS, the channel that showed highest activation was identified. The block averaged response for HbO, HbR and HbT were determined for the same channel of activation. For instance in figure 4.1 the encircled regions represent the highest channel of activation (X3O15) in the fNIRS data for one subject.

Each column in the NIRS data represents the activation maps for HbO, HbR and HbT signals. The columns in the fMRI data on the other hand represent activation in axial, sagittal and coronal planes. Each row in each of these figures represents the activation for the 2 s, 4 s, 8 s and16 s protocol. The location of the vitamin E capsules in each of the views of the fMRI data helps us identify the optical probe location in the MRI Scans. A couple of source detector positions have been marked on the fMRI data.

It can be clearly observed that the BOLD signal was consistently concentrated below the activated source-detector pairs in fNIRS. Hence, there is exists a fairly good spatial correlation between the two modalities.

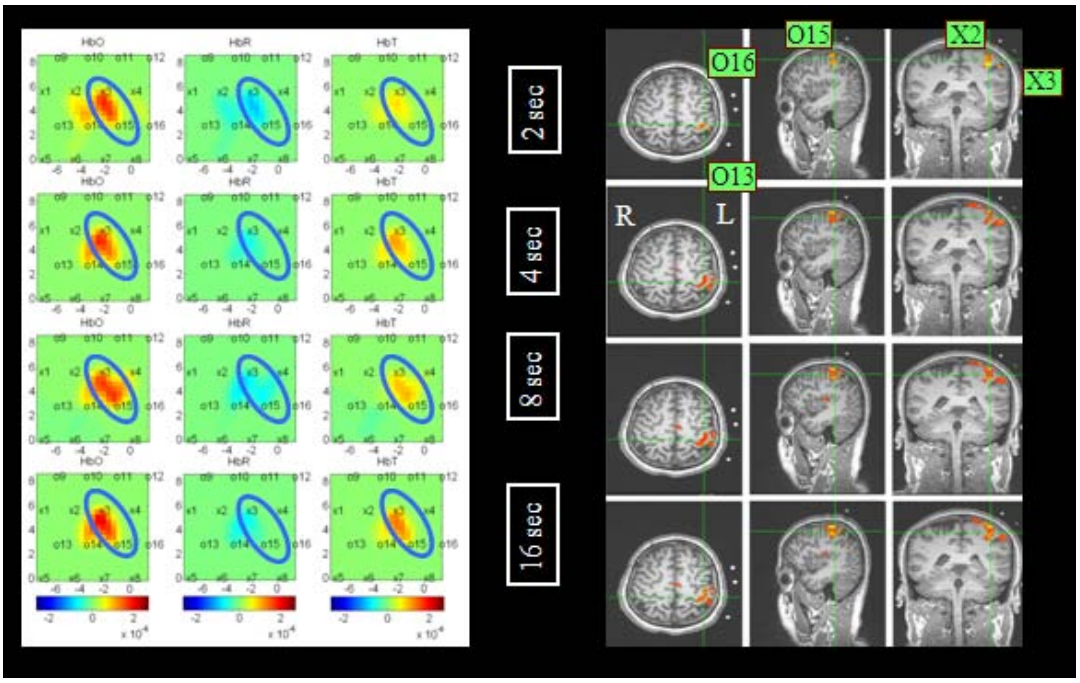

fNIRS fMRI

Figure 4.1: Spatial correlation of activation in NIRS and MRI

4.1.2 Temporal Response Correlation

Figure 4.2 shows the temporal profile of the block averaged data for the 2 s, 4 s, 8 s and 16 s protocol for a single subject (Subject 1). The plots represent the block averaged data for change in concentration of HbO (Figure 4.2(a)), HbR (Figure 4.2(b)), HbT (Figure 4.2(c)) and change in BOLD signal (Figure 4.2(d)) in a clockwise direction.

For the NIRS data the channel of highest activation for d[HbO], d[HbR] and d[HbT] (consistent among all the 4 protocols) is plotted and for the MRI data, the change in BOLD signal obtained after ROI averaging is plotted. The x axis represents the duration of the block for each protocol and the y axis the change in concentration (Molar) for HbO, HbR and HbT and the change in BOLD signal (a.u) respectively.

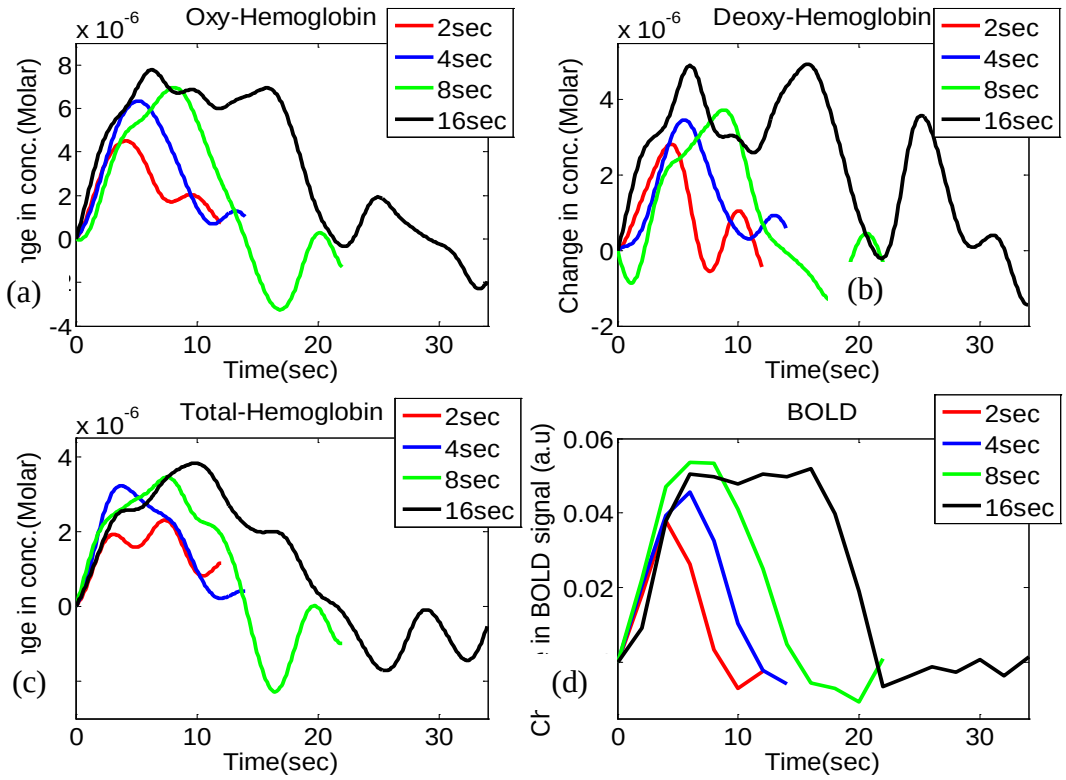

Figure 4.2: Subject 1 - Block Averaged Temporal Response (a) HbO; (b) HbR; (c) HbT; (d) BOLD signal

The amplitudes for all the parameters seem to increase with an increase in the duration of the stimulus and reach a plateau roughly after 4 seconds of motor task stimulus. The values of HbR plotted in this figure are inverted just for visual comparison.

Similar plots were obtained for Subject 2 as indicated in Figure 4.3. The results for Subject 2 are fairly consistent with Subject 1. The response amplitudes and the plateau affect appear to be similar in both subjects.

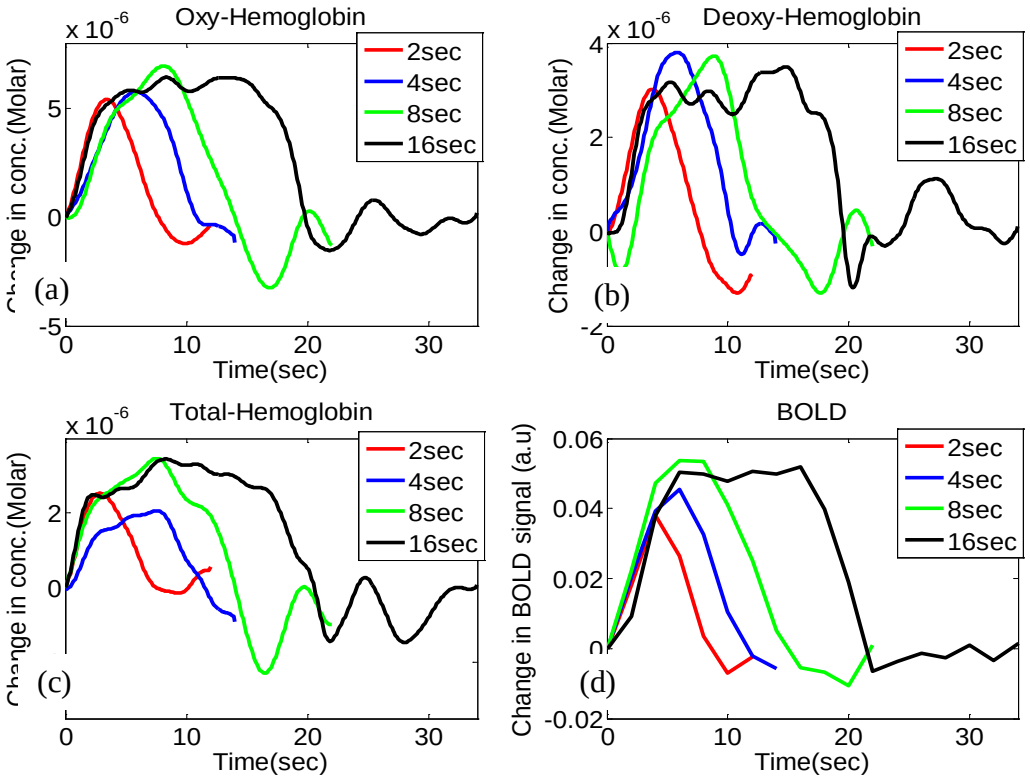

Figure 4.3: Subject 2 - Block Averaged Temporal Response (a) HbO; (b) HbR; (c) HbT; (d) BOLD signal

For Subject 3 however, there the activation in the NIRS data appeared to occur 2 seconds prior to the motor stimulus. This perhaps could be due to lack of synchronization in the start of the data acquisition period in both the imaging systems. This behavior was not observed in the BOLD signal. Hence in Figure 4.4, the NIRS data represents block averaged data from 2 seconds before the stimulus. For subject 3, the change in concentration of HbO and HbR seems to an order of a magnitude higher than that of Subject 1 and Subject 2. Also the change in concentration of the HbO signal has an extremely poor signal to noise ratio. This could be due to poor contact established between the probe and the scalp of the subject.

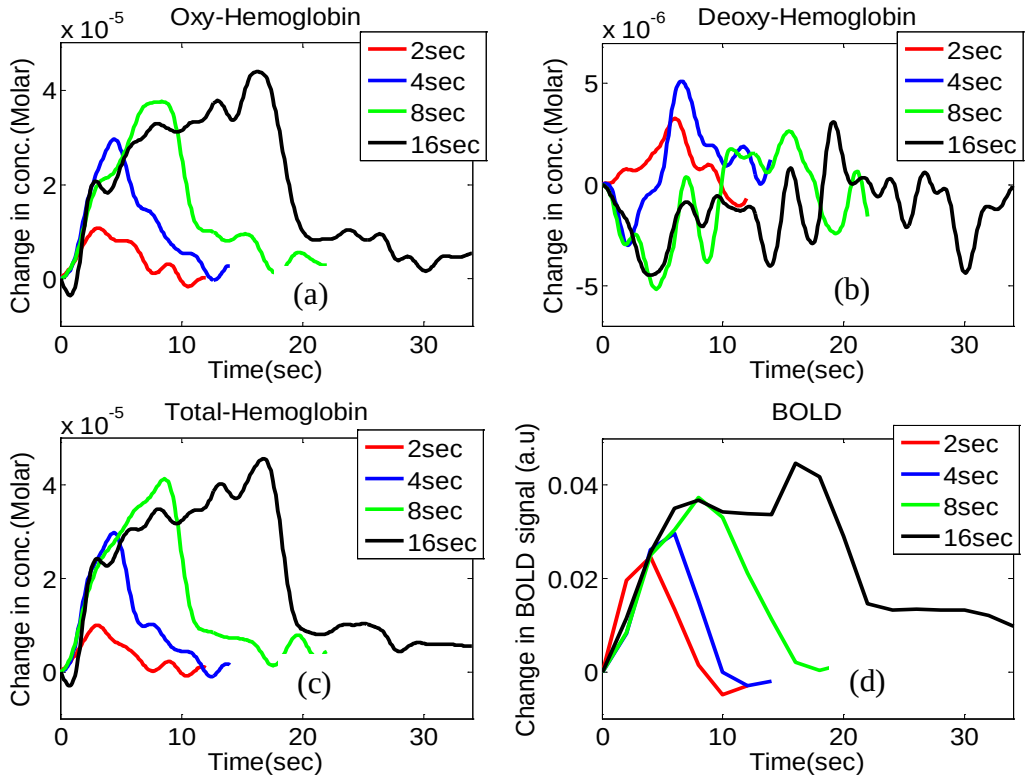

Figure 4.4: Subject 3 - Block Averaged Temporal Response (a) HbO; (b) HbR; (c) HbT; (d) BOLD signal

The temporal response of all the subjects was averaged and plotted together to check for the consistency in temporal profiles across the modalities at the group level (Figure 4.5).

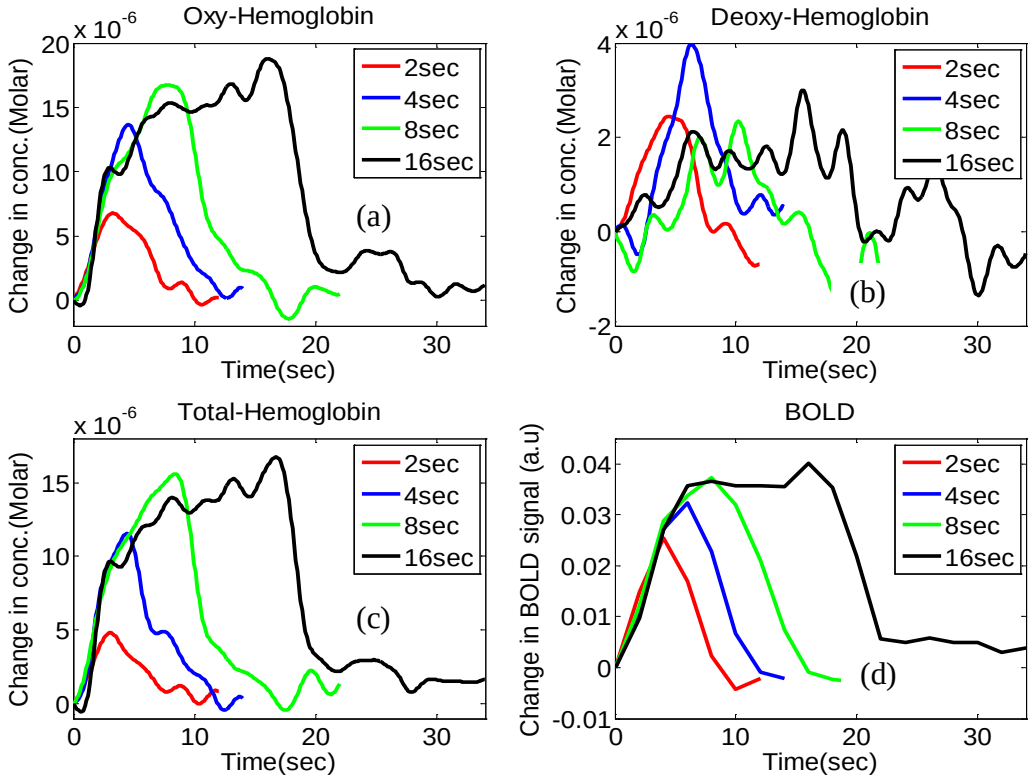

Figure 4.5: Average of subjects - Block Averaged Temporal Response (a) HbO; (b) HbR; (c) HbT; (d) BOLD signal

Although the temporal profiles across the modalities even at the group level seem to be fairly consistent, it is hard to conclude whether the BOLD signal correlates most to the HbO, HbR or the HbT signal.

As the scales of HbO, HbR and HbT differ from that of BOLD to estimate a correlation between these parameters it was essential to normalize the data between a scale of 0 and 1. The normalized block averaged data across the 3 subjects is represented in Figure 4.6. The graphs in the clockwise direction indicate the normalized data for the 2 s (Figure 4.6(a)), 4 s (Figure 4.6(b)), 8 s (Figure 4.6(c)) and 16 s (Figure 4.6(d)) motor task paradigm. Each graph represents the normalized for HbO, HbR, HbT and the BOLD signal.

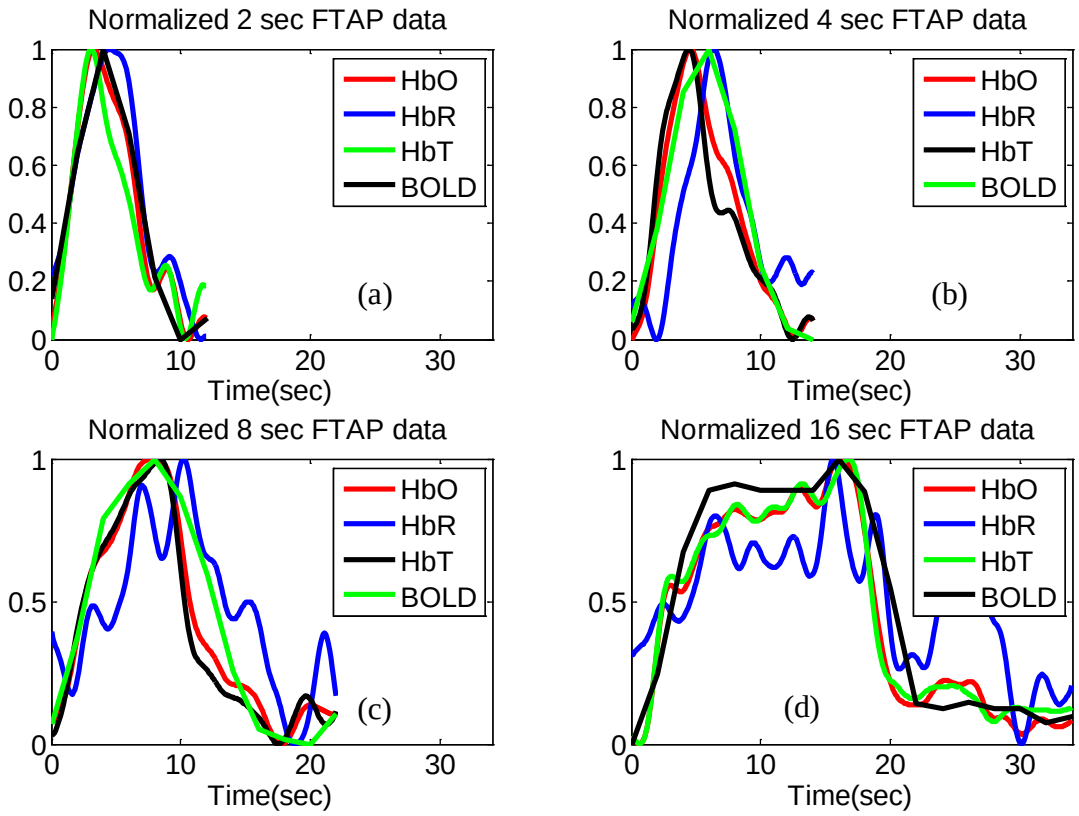

Figure 4.6: Average of subjects – Normalized Block Averaged Temporal Response for HbO, HbR, HbT and BOLD signal (a) 2 s; (b) 4 s; (c) 8 s; (d) 16 s

In order to identify what parameter of blood (HbO, HbR an HbT) the BOLD signal correlates to the most, the signals were normalized between a scale of 0 and 1. Then the Pearson Correlation Coefficient 'R' was calculated of the BOLD signal with each of the HbO, HbR and HbT signals. The correlation coefficients were calculated for each subject individually and for the average of all the subjects. Figure 4.6 shows the correlation coefficients of the BOLD signal with HbO, HbR and HbT for each subject individually and the average of all the subjects for the 2 second protocol.

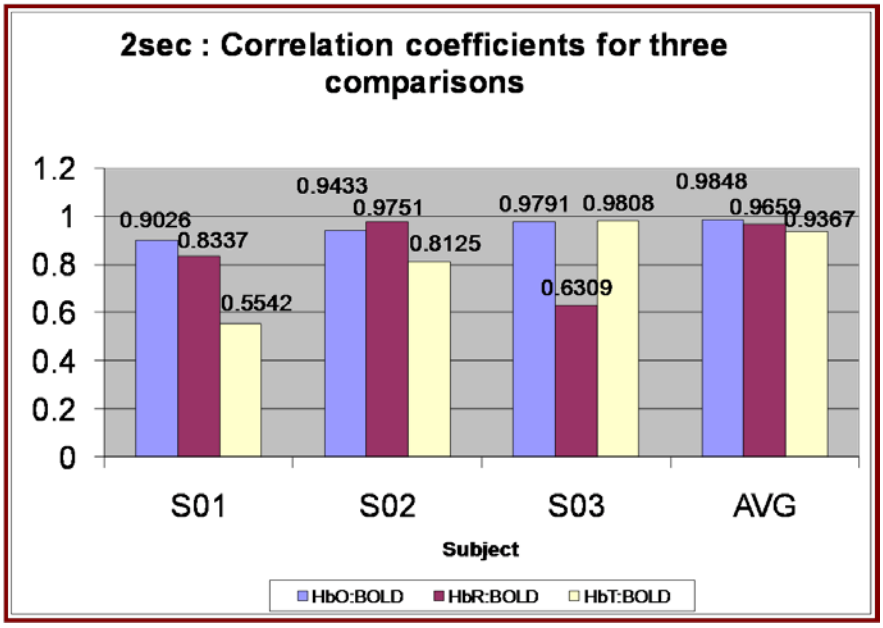

Figure 4.7: 2 sec protocol - Correlation coefficients of HbO: BOLD, HbR: BOLD and HbT: BOLD

The Pearson correlation coefficient (R) value of HbO: BOLD is obtained to be higher in general for the subjects individually and at the group level in comparison to the R value for HbR: BOLD and HbT: BOLD.

Similarly the R values were obtained for the 4 s, 8 s and the 16 s protocol. These values are shown in Figure 4.7, 4.8 and 4.9 respectively. All 4 paradigms showed highest correlation of HbO with BOLD signal in comparison to HbR with BOLD signal and HbT with BOLD signal. In Subject 3, the correlation of HbO with BOLD is extremely low. We expect this de-oxy hemoglobin signal obtained for Subject 3 is extremely noisy

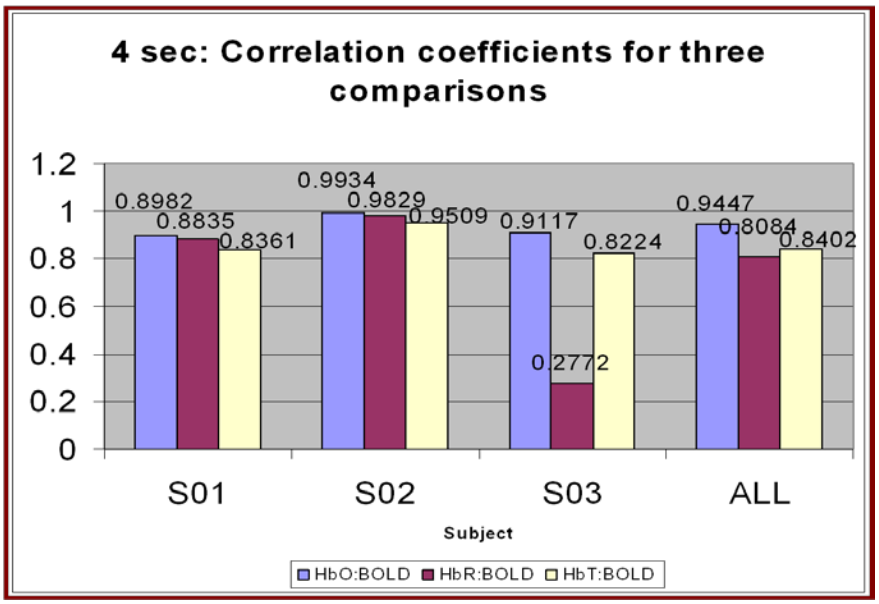

Figure 4.8: 4 sec protocol - Correlation coefficients of HbO: BOLD, HbR: BOLD and HbT: BOLD

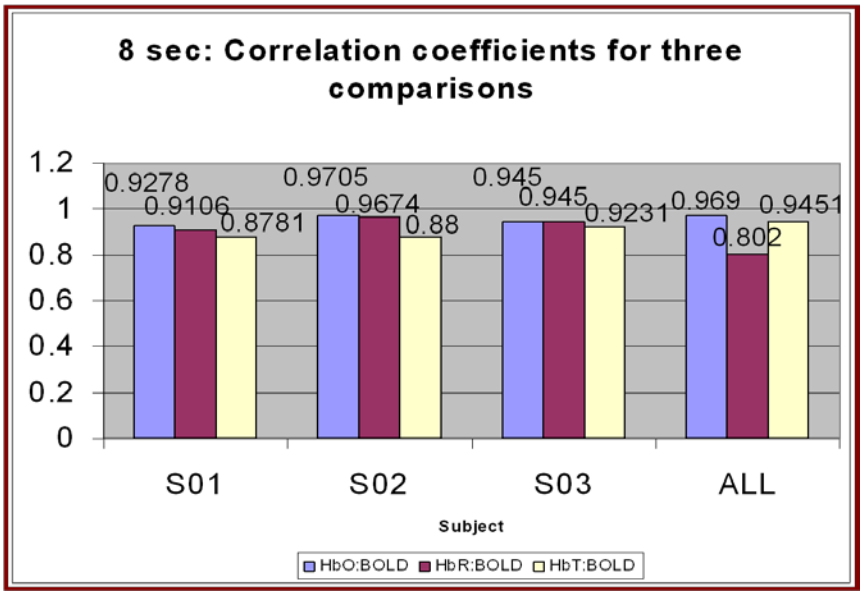

Figure 4.9: 8 sec protocol - Correlation coefficients of HbO: BOLD, HbR: BOLD and HbT: BOLD

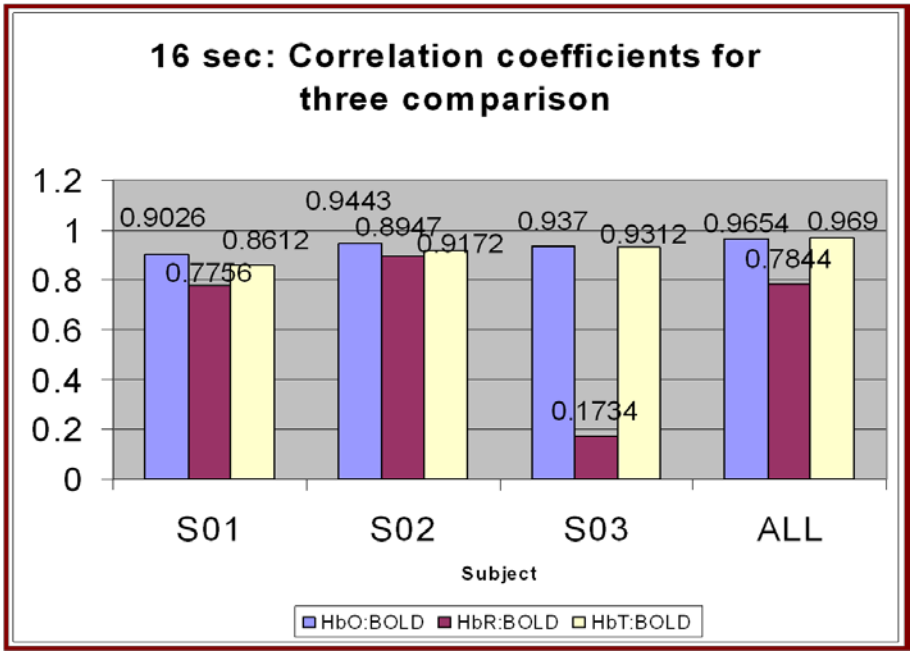

Figure 4.10: 16 sec protocol - Correlation coefficients of HbO: BOLD, HbR: BOLD and HbT: BOLD

4.2 Phenomenological Properties

It is very important to examine certain characteristic features (phenomenological parameters) of a curve in order to compare and contrast it with another curve. As a part of phenomenological parameters, the maximum amplitude ratios and the full width half maximum ratios of 4 sec, 8 sec and 16 sec protocols have been compared as ratios with respect to the 2 sec protocol. The graph below indicates the ratio of the max amplitude of the 4, 8 and 16 seconds protocol with respect to the 2 second protocol.

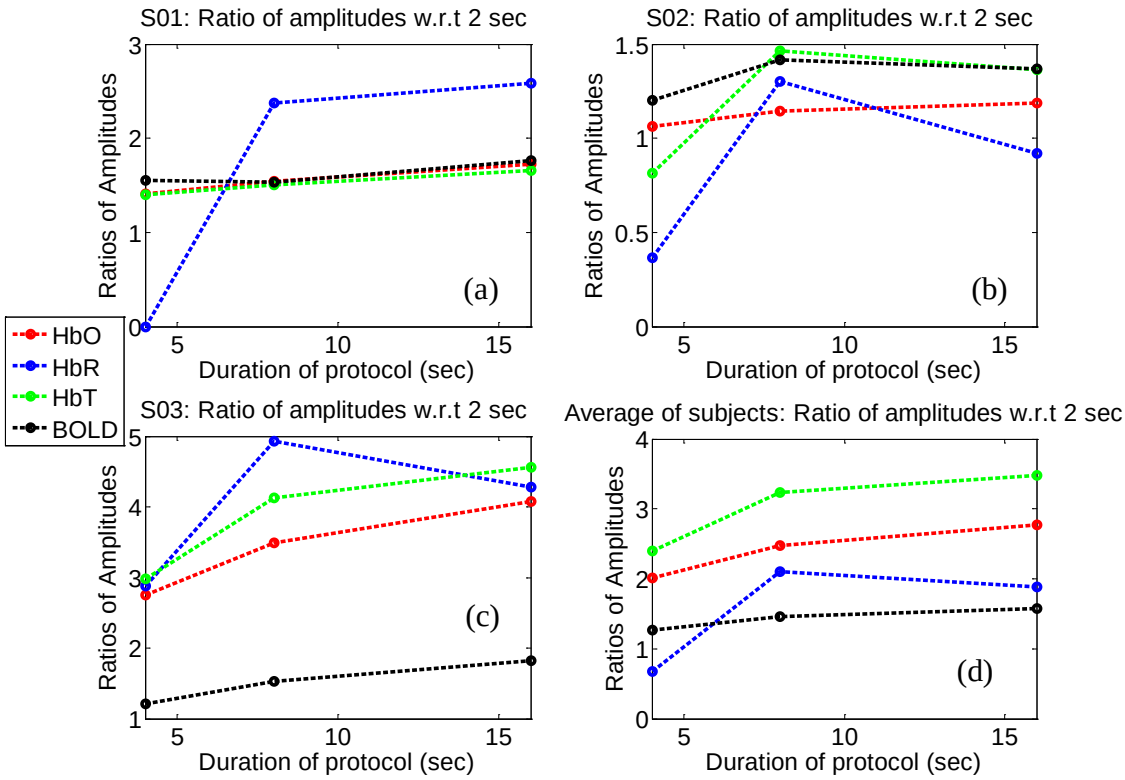

Figure 4.11: Maximum amplitude vs Duration (a) S01, (b) S02, (c) S03, (d) Average of Subjects

As the maximum amplitude is in reference only to one value at one point, the full width half maximum which in a way measures the area under the curve is considered to be a more reliable way to compare and contrast 2 curves. The next graph below indicates the ratio of the full width half max of the 4, 8 and 16 seconds protocol with respect to the 2 second protocol.

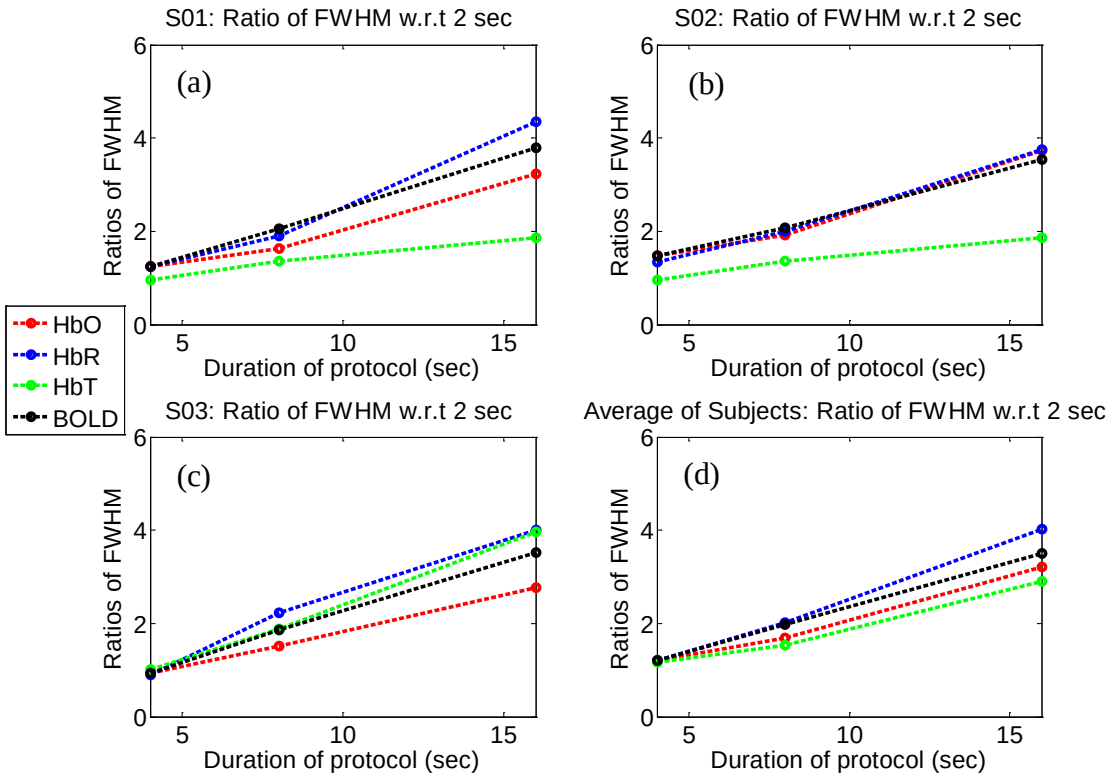

Figure 4.12: FWHM vs Duration (a) S01, (b) S02, (c) S03, (d) Average of Subjects

4.3 Nonlinearity

Figure 4.13 indicates non-linearity in the BOLD signal for Subject 1. The stimulus duration on the x-axis is used to predict the stimulus duration on the y-axis. The blue curve indicates the measured response and the red curve indicates the predicted response. Shorter stimulus durations are shifted in time to predict longer stimulus durations (a multiple of the shorter stimulus duration). For example, in the first column, 2s stimulus is used to predict the 4 s, 8 s and the 16 s stimulus. Similarly, non-linearity in HbO (Figure 4.14), HbR –inverted (Figure 4.15) and HbT (Figure 4.16) for Subject 1 have been plotted.

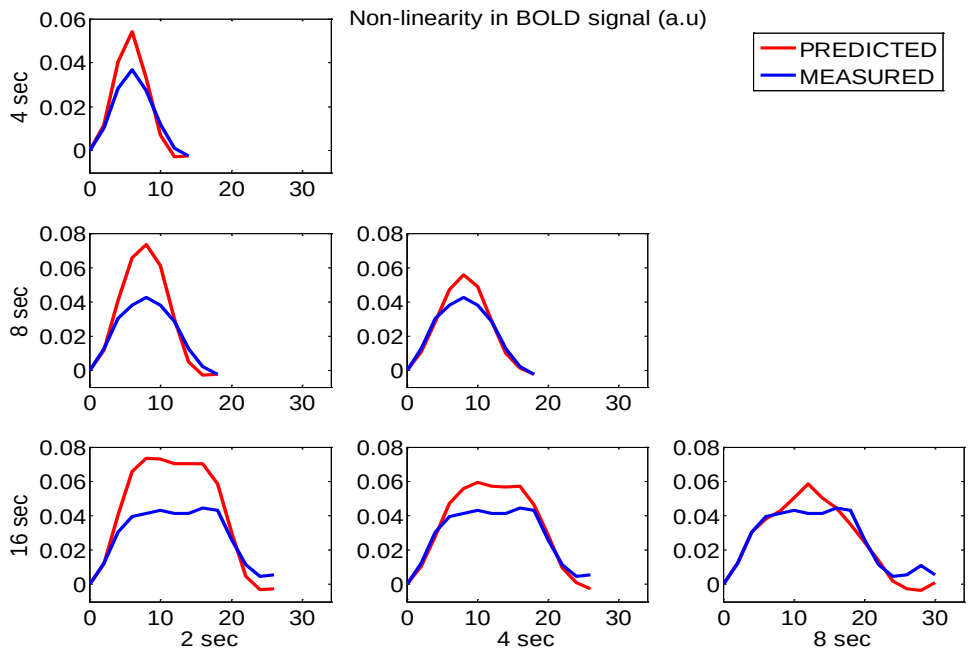

Figure 4.13: Subject 1 - Non-linearity in BOLD signal (a.u.)

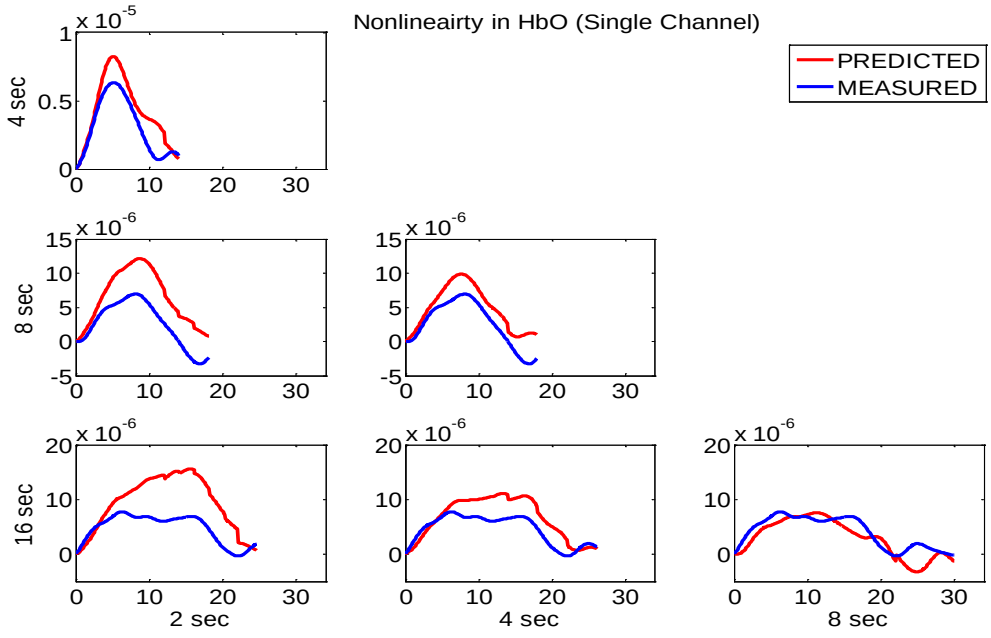

Figure 4.14: S01: Non-linearity in HbR

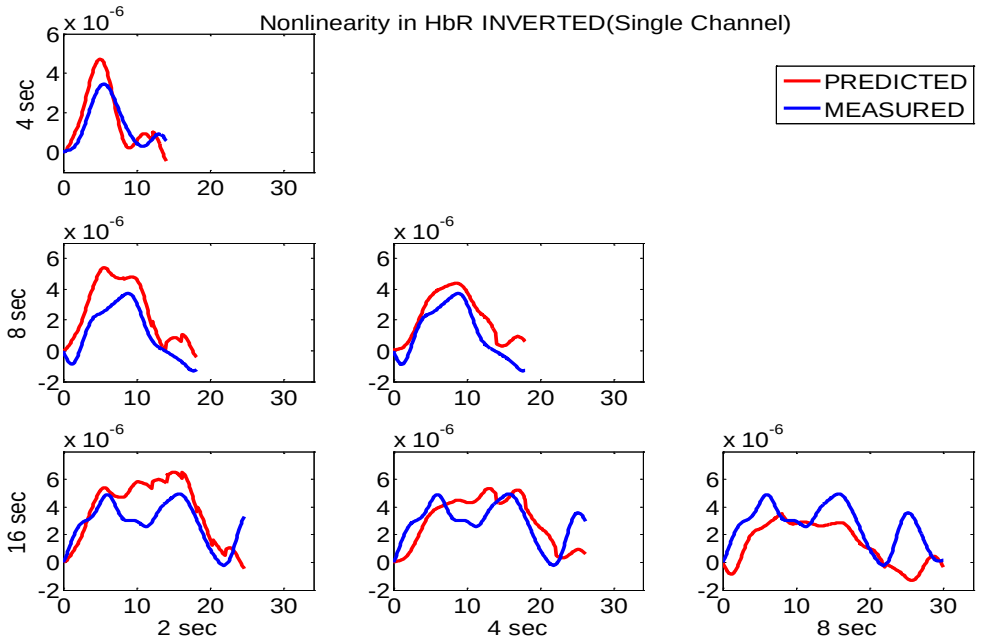

Figure 4.15: Subject 1: Non-linearity in HbT

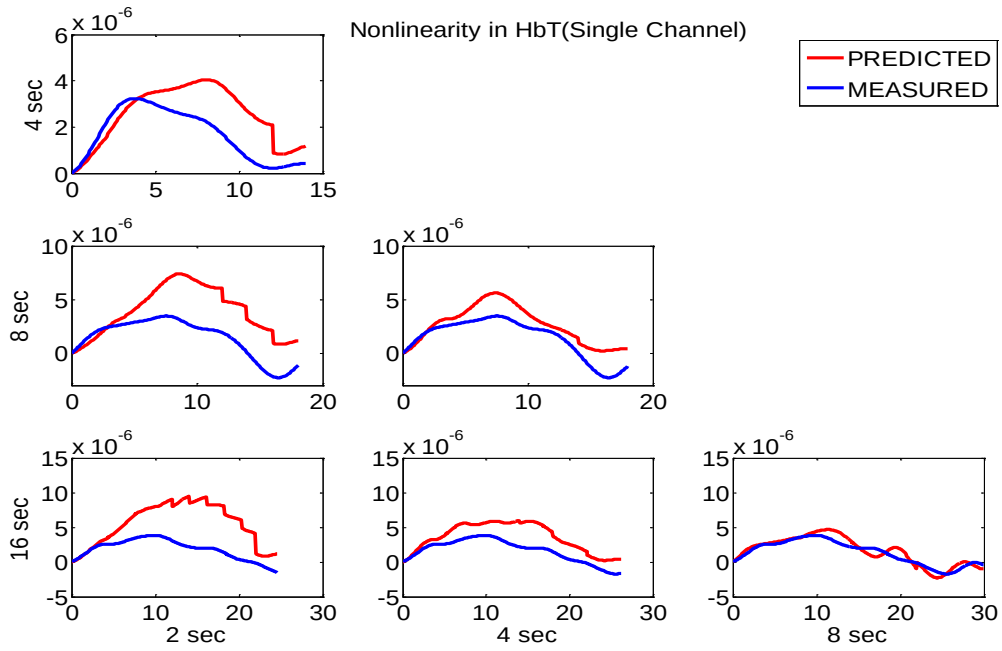

Figure 4.16: Subject 1: Non-linearity in BOLD

The four figures above show the non-linearity of fNIRS data: HbO, HbR, HbT and BOLD signals with a longer stimulation period are estimated by adding several shorter-stimulus responses. As clearly shown, the estimated responses based on multiple shorter-duration stimuli over-estimate the actual long-stimulus response, whereas the estimates using longer duration responses fit better for HbO, HbR, HbT and BOLD.

The next four figures represent non-linearity in BOLD (Figure 4.17), HbO (Figure 4.18), HbR-inverted (Figure 4.19) and HbT (Figure 4.20) for Subject 2. In Subject 2 like in Subject 1, the non-linearity seems to exist at shorter stimulus durations where the predicted response overshoots the measured response to a larger extent than at longer stimulus durations. Hence, the results of nonlinearity of Subject 2 are more or less consistent with the nonlinearity seen in Subject 1.

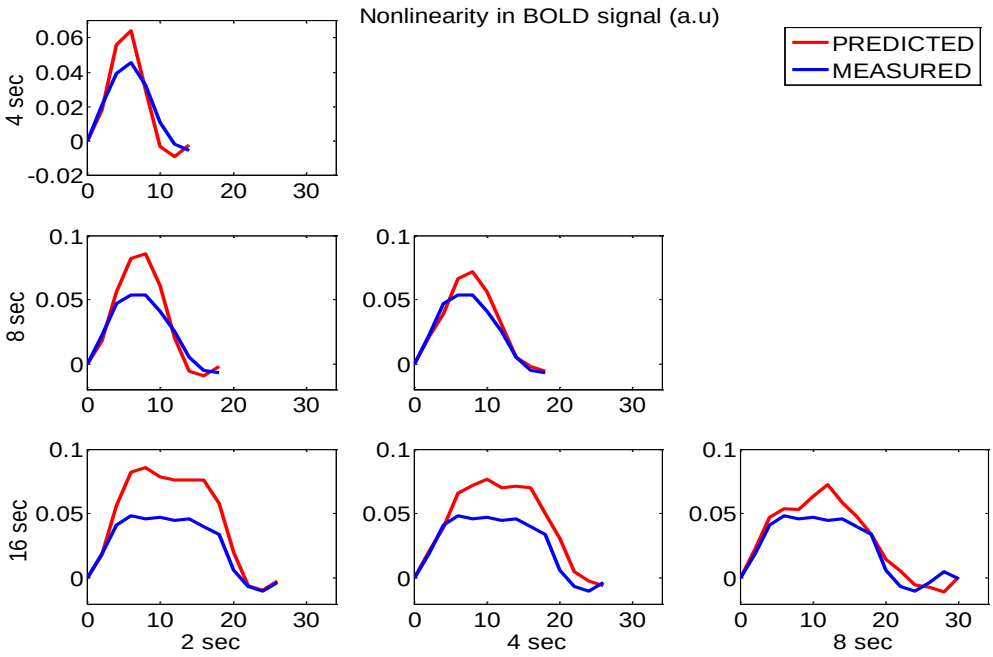

Figure 4.17: Subject 2 - Non-linearity in BOLD signal (a.u.)

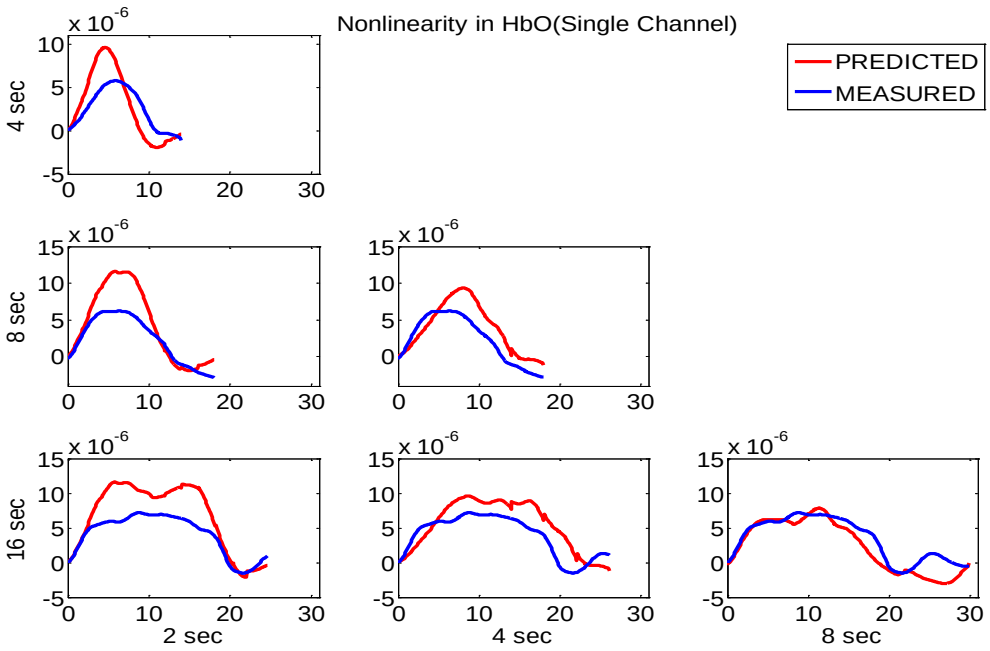

Figure 4.18: Subject 2 - Non-linearity in HbO (Molar)

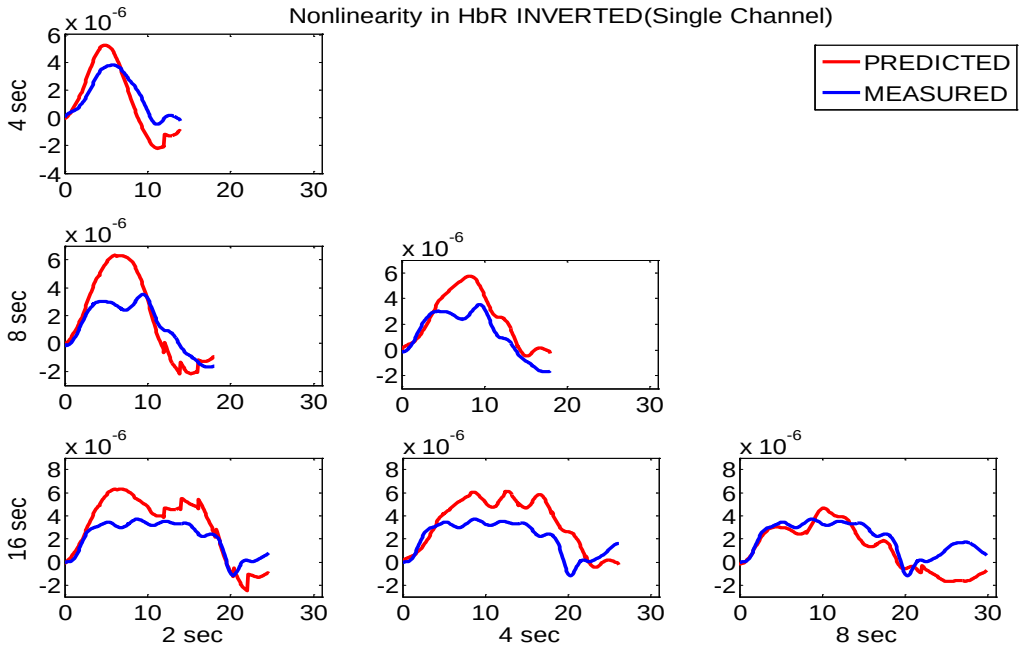

Figure 4.19: Subject 2 - Non-linearity in HbR - inverted (Molar)

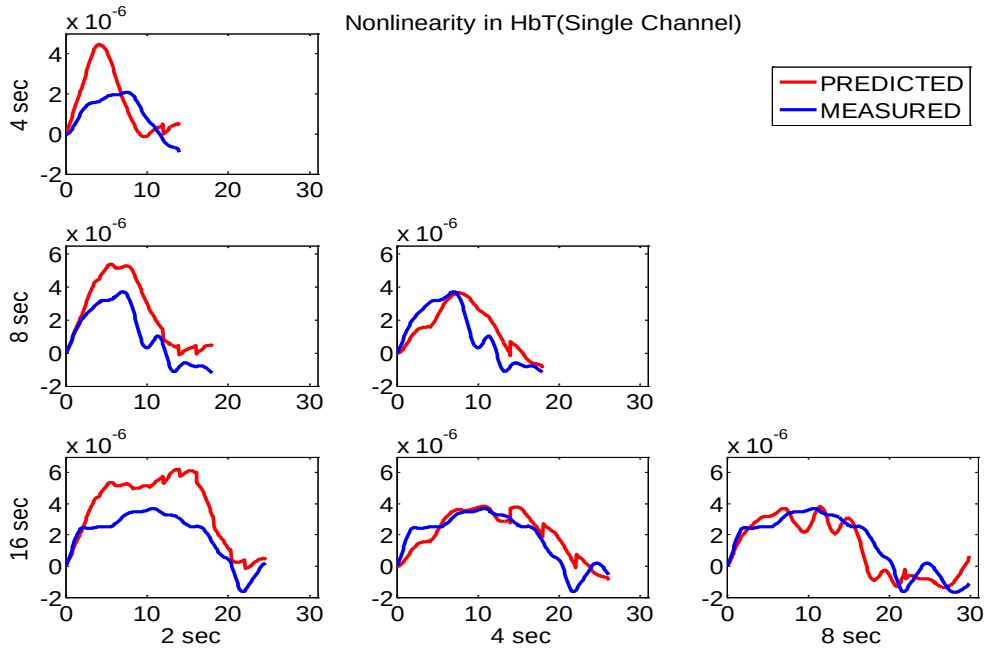

Figure 4.20: Subject 2 - Non-linearity in HbT (Molar)

The next four figures represent non-linearity in BOLD (Figure 4.21), HbO (Figure 4.22), HbR-inverted (Figure 4.23) and HbT (Figure 4.24) for Subject 3. In Subject 3, nonlinearity is not evident in both modalities. As Subject 3, does not show any non-linearity, it has not been included in the averaged data for nonlinearity. Average data for nonlinearity in Subject 1 and Subject 2 is shown in Figure 4.25 (BOLD), Figure 4.26 (HbO), Figure 4.27(HbR), and Figure 4.28 (HbT). The data averaged across the 2 subjects shows nonlinear behavior at shorter stimulus durations and becomes more linear at longer stimulus durations.

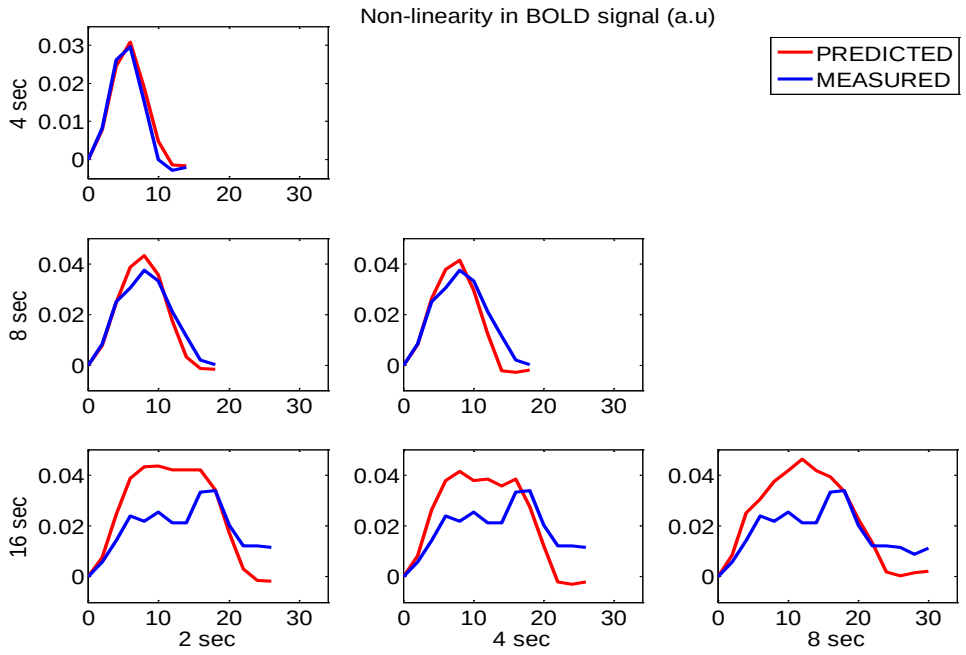

Figure 4.21: Subject - 3: Non-linearity in BOLD Signal (a.u.)

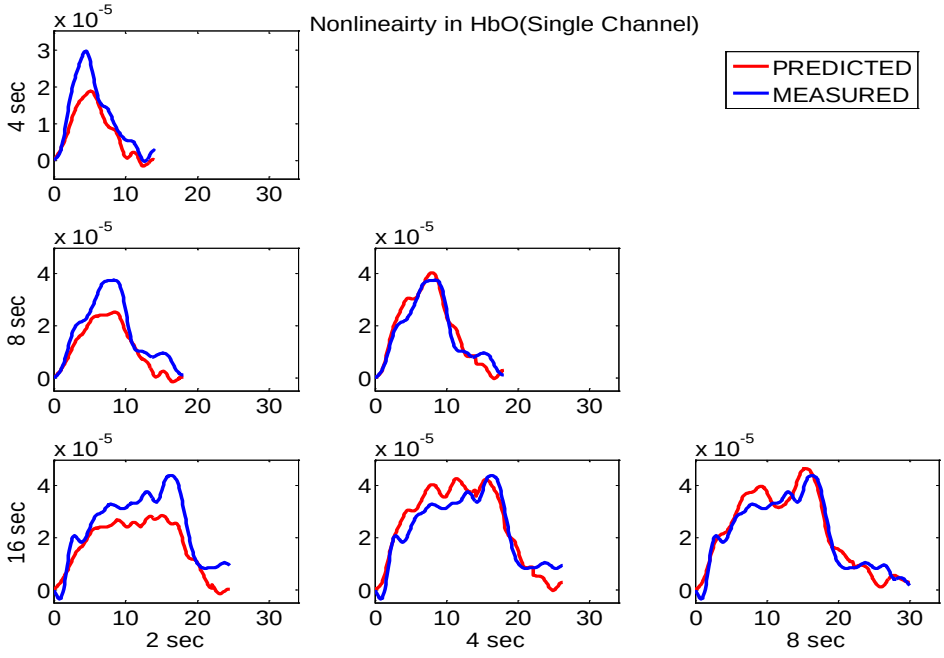

Figure 4.22: Subject 3 - Non-linearity in HbO (Molar)

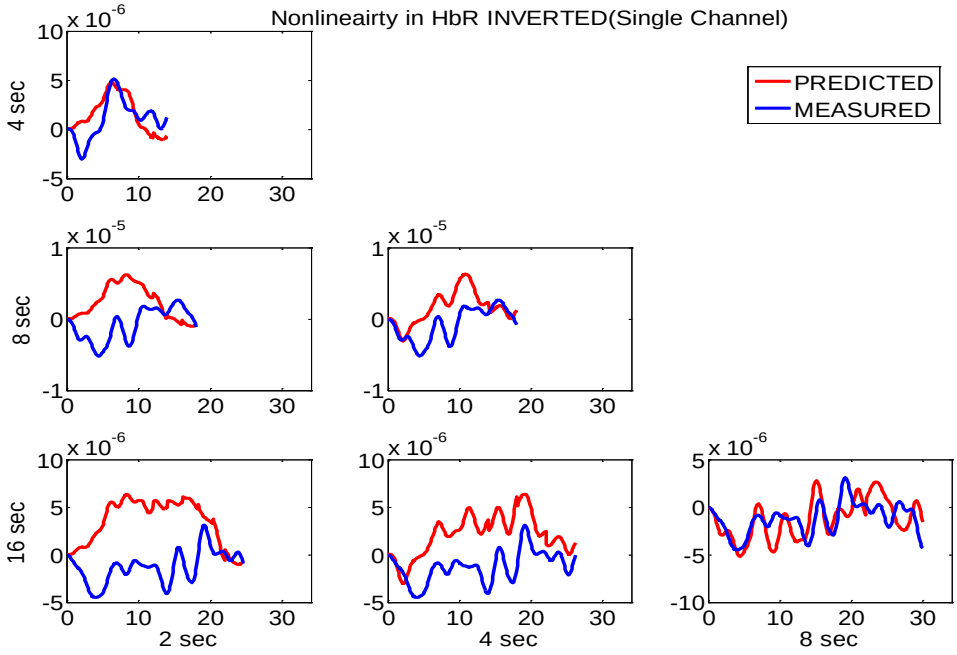

Figure 4.23: Subject 3 - Non-linearity in HbR - inverted (Molar)

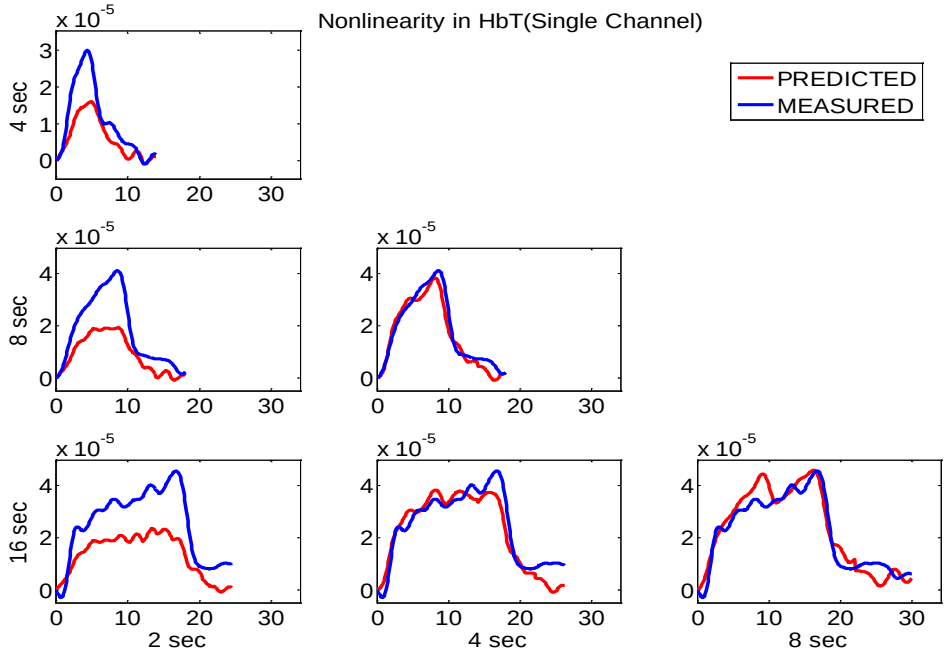

Figure 4.24: Subject 3- Non-linearity in HbT (Molar)

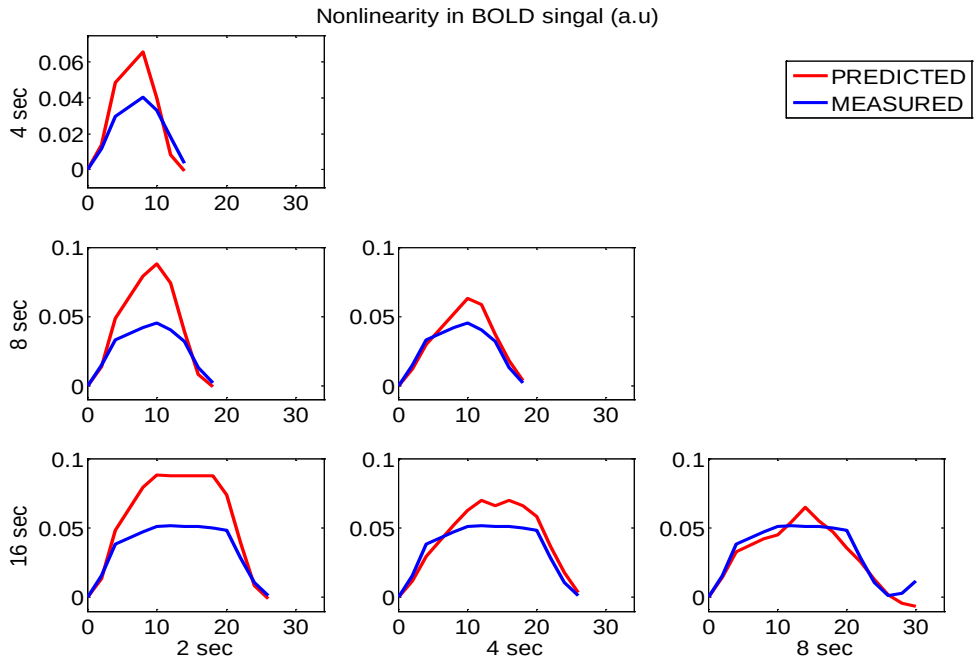

Figure 4.25: Subject 3 - Non-linearity in BOLD signal (a.u)

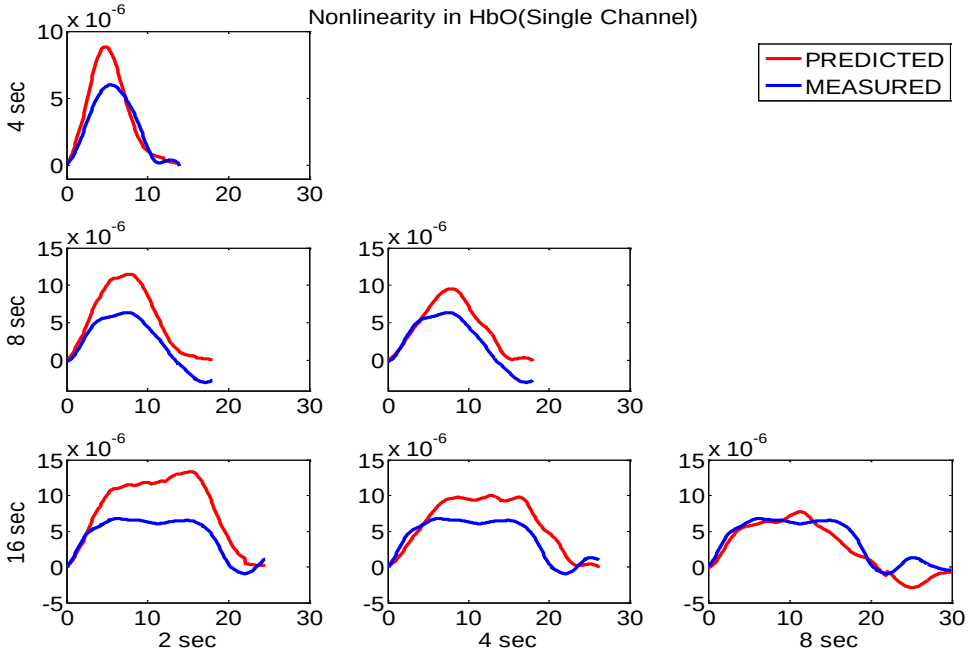

Figure 4.26: Average of subjects - Non-linearity in HbO (Molar)

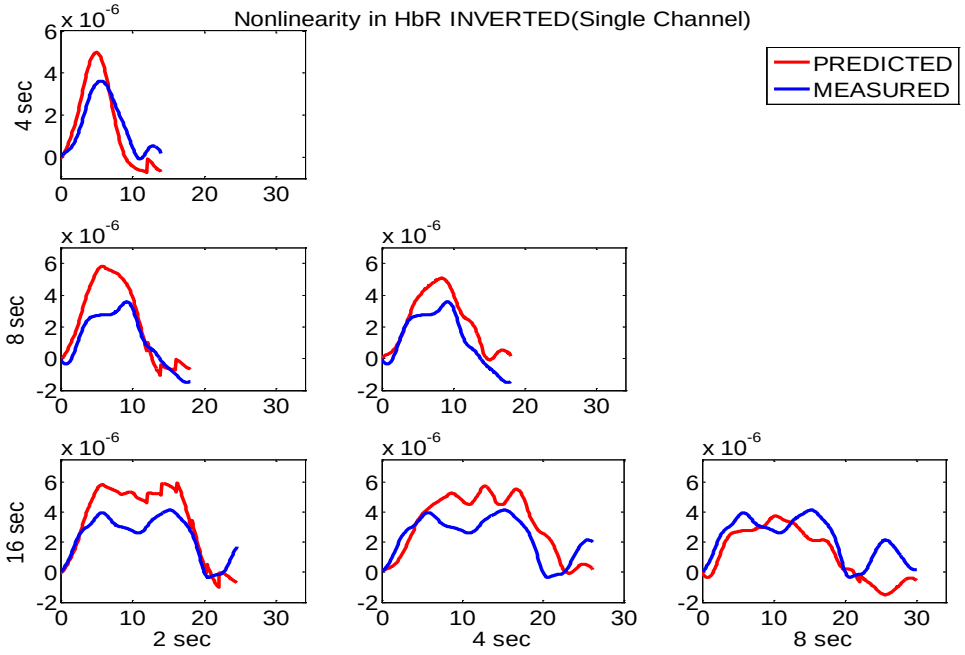

Figure 4.27: Average of subjects - Non-linearity in HbR - inverted (Molar)

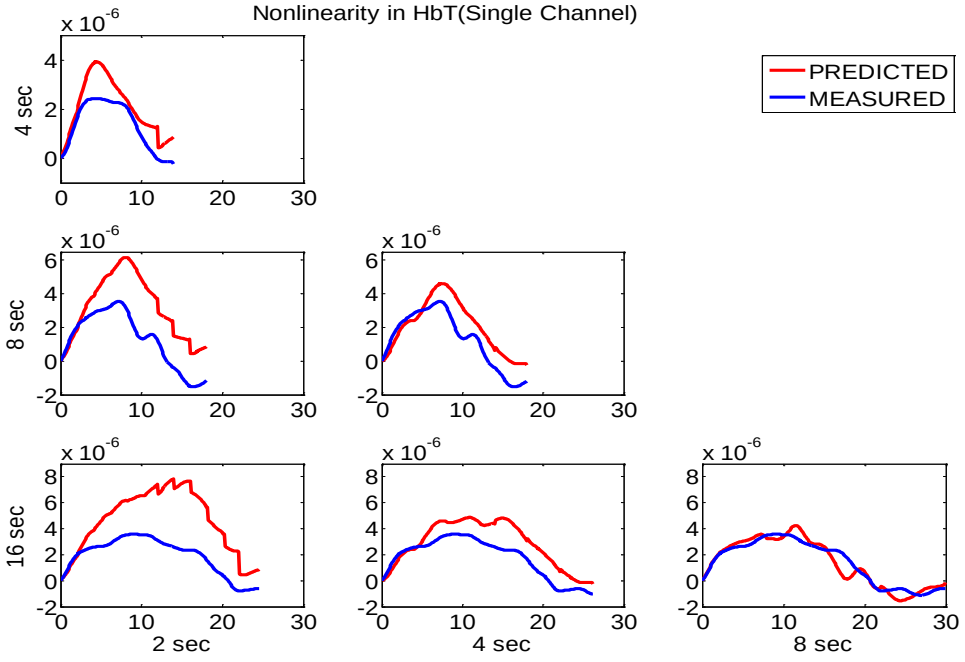

Figure 4.28: Average of subjects - Non-linearity in HbT (Molar)

The root mean square errors (RMSE) between the estimated and actual response were calculated and normalized in order to see the goodness of fit as well as the differences in three hemodynamic parameters. The calculated errors do support the non-linearity observed in the curves. The RMSE of average response of all the subjects put together shows that over estimated responses are obtained by adding the responses taken from smaller stimulus durations for HbO, HbR, HbT and BOLD

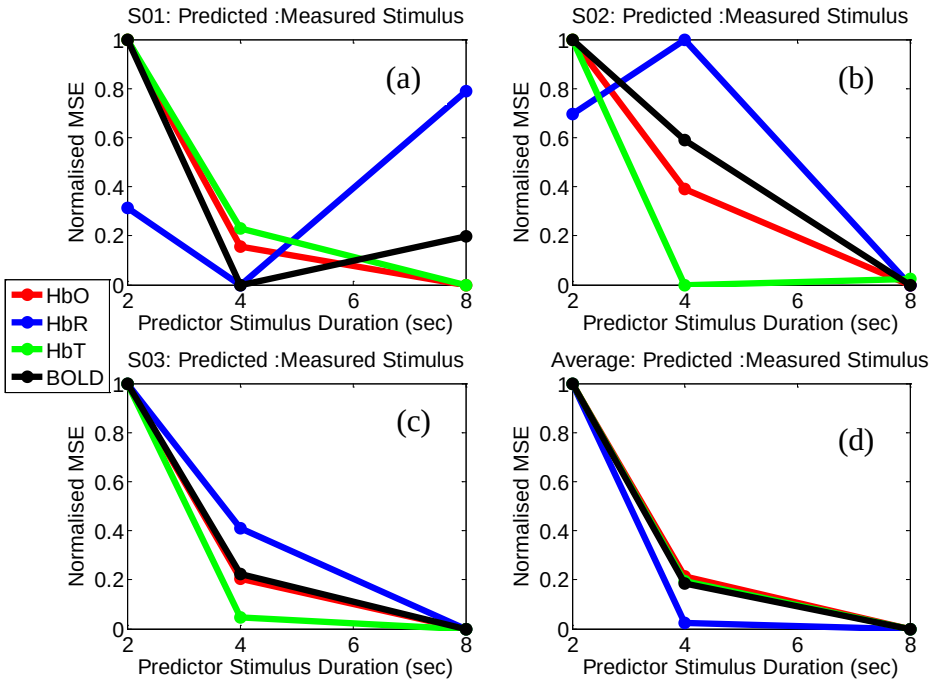

Figure 4.29: Normalized Predicted vs Measured Stimulus Duration

4.4 Modeling Hemodynamic Response

Non-linearity as mentioned earlier is believed to be due to neural adaptation amongst other factors. Hence, when modeling the hemodynamic response, neural adaptation definitely has to be

accounted for. Based on literature [10], neural adaptation is modeled as a two parameter exponential equation.

$$n(t) = 1+a*e^{(-t/b)}$$

where 'a' represents the initial offset in neuronal firing

'b' represents decay constant

The hemodynamic response has been modeled to fit for a 3 parameter gamma variate function.

$$i(t) = c1*(t/c2)^{c3}*e^{(-t/c2)}$$

where 'c1' affects the amplitude of the response

'c2' affects the time to peak and full width half maximum of the response.

'c3' affects the time to peak and the amplitude of the response.

A second test of linearity is performed by using the algorithm discussed here. A rectangular stimulus function is multiplied with the neural adaptation function described above. The resultant function is then convolved with the hemodynamic response function also described above. The convolved response is then fitted to the measured response. This model was used for both the fNIRS and the fMRI data. Figure 4.30 represents a graphical display of the algorithm for a 16 sec stimulus and its measured response. The rectangular stimulus function is represented as '1' for the task period and '0' for the rest period. Hence, this function varies depending on the duration of the protocol. For the fNIRS data this function is represented in seconds. For the fMRI data this function is represented in TR's.

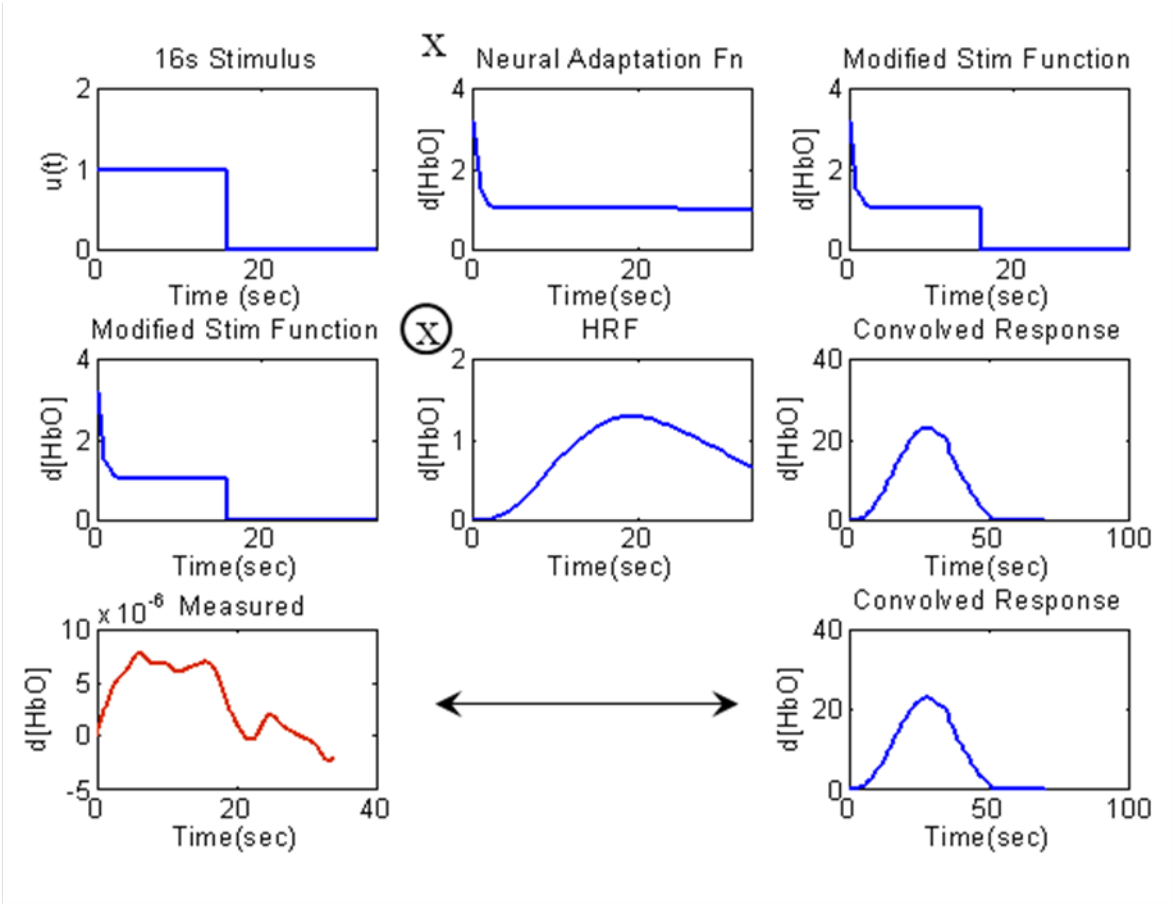

Figure 4.30: Algorithm for modeling hemodynamic response

The modeling algorithm was implemented using the *'lsqcurvefit'* function in Matlab. This function solves non-linear least square problems. The input parameters to be specified for this function are the time scale, the data to be fitted, the measured data, the starting estimates of all five parameters (a, b, c1, c2, c3) and the lower and upper bounds within which the solution set of the parameters should lie. These lower and upper bound were specified based on existing values [10]. It is important to specify these bounds so that the solutions lie within a range to which physiological meaning can be added. The algorithm find a fit where the least square error between the measured and the fitted data is minimum for a default number of iterations.

As the most robust fNIRS signal obtained in this study is HbO, as a preliminary step the fitting algorithm has been used only for change in HbO (Molar) and change in BOLD signal (a.u.). Figure 4.31 shows the measured and the fitted response obtained from the algorithm described above for the 2 sec, 4 sec, 8 sec and the 16 sec finger tapping protocol for the fNIRS data for Subject 1. The x axis represents the time in seconds and the y axis represents the change in HbO (Molar). The blue and green curves in each graph represent the measured and fitted fNIRS data respectively.

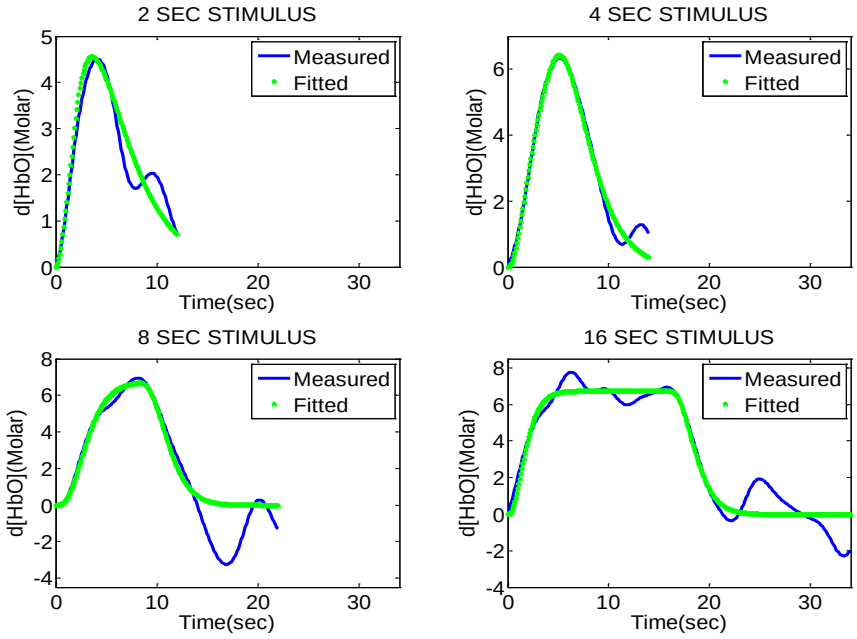

Figure 4.31: Subject 1: NIRS modeled hemodynamic response

Visually, the algorithm seems to fit well for the 2 s, 4 s, 8 s and the 16 s protocol. Similarly these graphs were obtained for the fMRI data of Subject 1 as shown in Figure 4.32. The x axis represents the time in seconds (TR's have been converted to seconds for consistency across both modalities) and the y axis represents the change in BOLD signal (a.u). The blue and

green curves in each graph represent the measured and fitted fMRI data respectively. This model visually, also seems to fit well in this case.

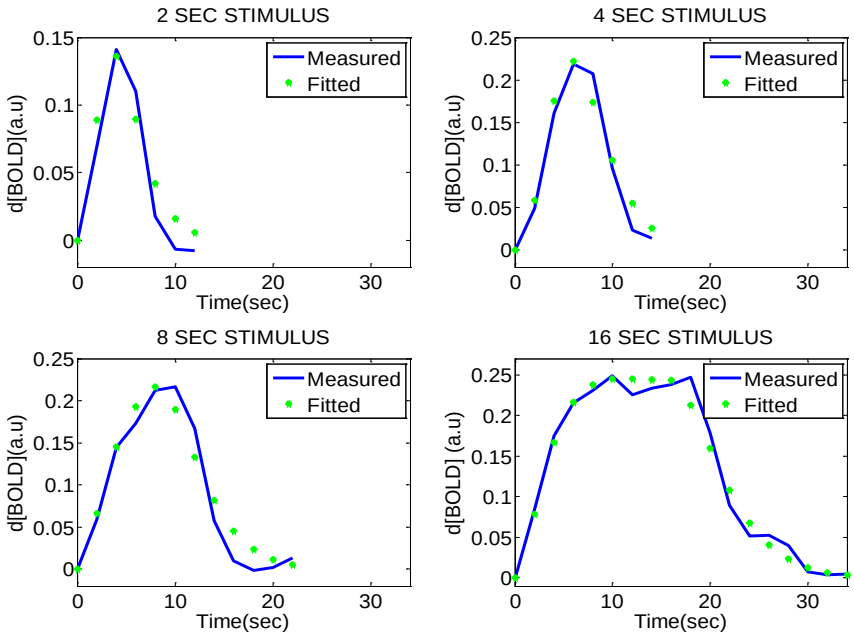

Figure 4.32: Subject 1: BOLD modeled hemodynamic response

These graphs were modeled for Subject 2 as well. Figure 4.33 and Figure 4.34 show the measured and fitted graphs for the fNIRS data and fMRI data respectively. The algorithm seems to fit well for Subject 2's data set. For both Subject 1 and Subject 2 a significant undershoot in observed in the 8 s fNIRS data. The algorithm discussed in detail above does not account for this undershoot. However, this undershoot is not observed in the fMRI data. The reason for these undershoot is unknown but occurs at various instances.

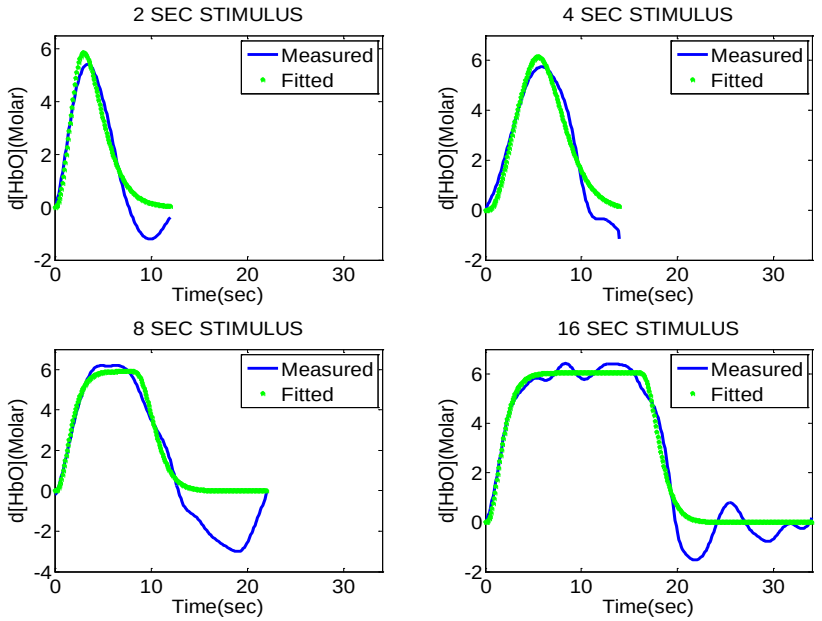

. Figure 4.33: Subject 2: NIRS modeled hemodynamic response

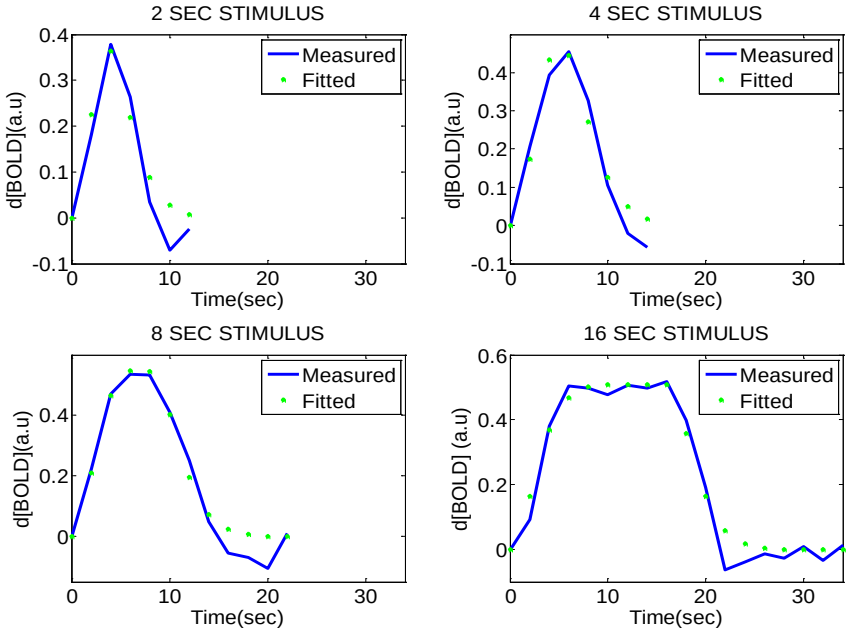

Figure 4.34: Subject 2: BOLD modeled hemodynamic response

These curves are also obtained for Subject 3's fNIRS and fMRI data as shown in Figure 4.35 and 4.36 respectively. Though the algorithm fits well for Subject 3, it does not account for noise that occurs at several points in the measured response.

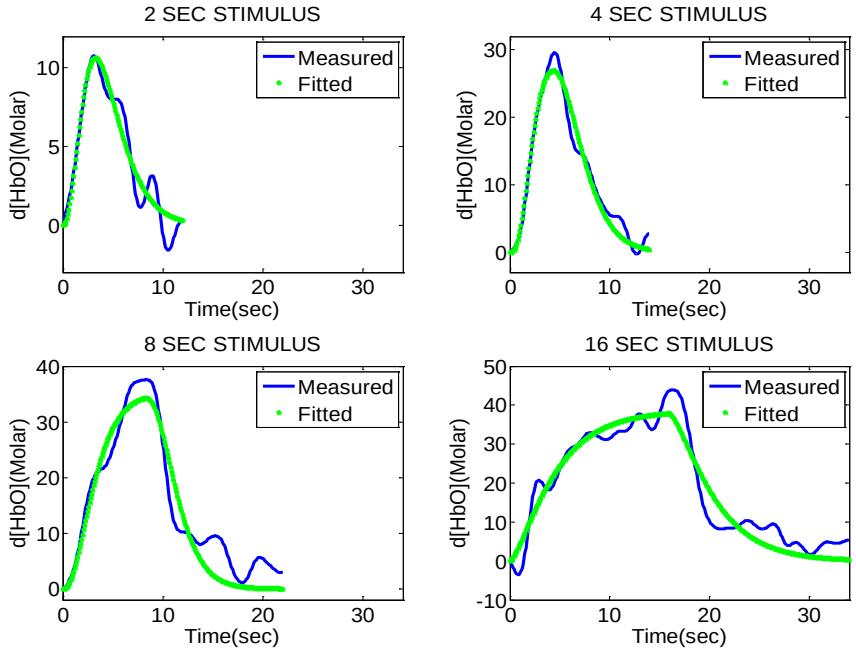

Figure 4.35: Subject 3 - HbO modeled hemodynamic response

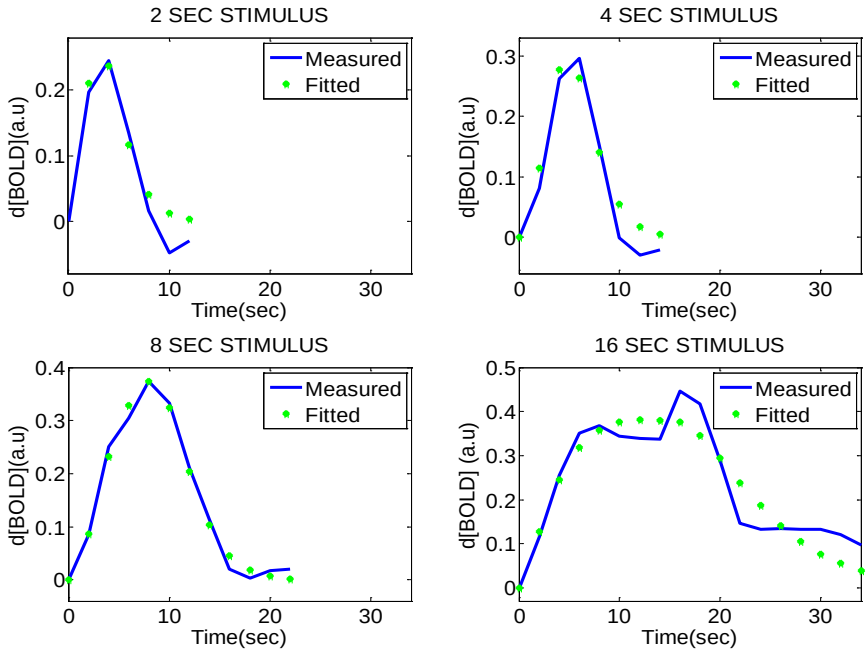

Figure 4.36: Subject 3 - BOLD modeled hemodynamic response

As the neural adaptation factor varies from an individual to individual, the results of this model being used for averaged data of 3 subjects is not shown. However using the '*lsqcurvefit*' function the values of the parameters (a, b, c1, c2 and c3) obtained are displayed in Figure 4.37. In Figure 4.37, the values of the fNIRS and fMRI parameters with their standard deviations averaged across the 2 s, 4 s, 8 s and 16 s protocols for the 3 subjects are shown. A student t-test was carried out to see is the parameter obtained for the fNIRS and the fMRI data were significantly different or not. The p-values obtained for each parameter are indicated on the graph (Figure 4.37).

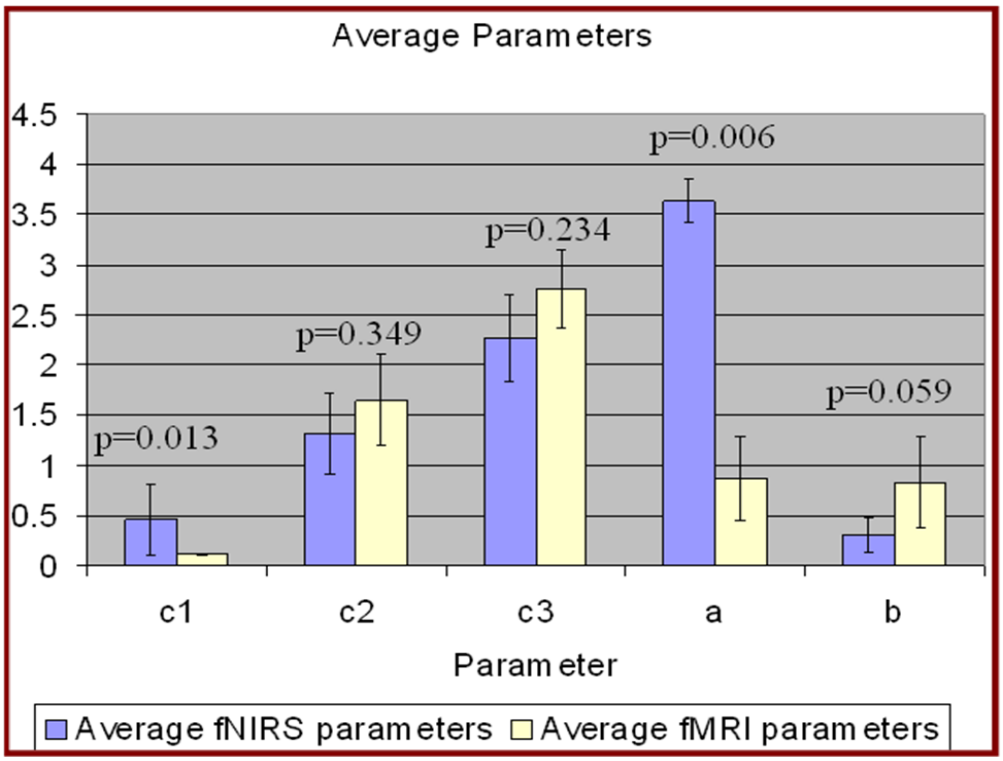

Figure 4.37: Hemodynamic response model parameters

The values indicate that the parameters obtained for the fNIRS and fMRI data are significantly different for c1 and a. The reason for this small variation is unknown. The values obtained for c2, c3 and b though, seem to be fairly consistent across both modalities.

4.5 Breath Hold Protocol Study

The breath hold data was implemented as a calibration standard across both the imaging modalities. Breath Hold protocol show global changes in the brain when performed [22]. Previous fNIRS studies have indicated signature activation due to breath hold protocols in the prefrontal cortex. All the data analyzed was analyzed at the same location as the finger tapping data to ensure consistency. The results are shown next. Figure 4.38 and Figure 4.39 shows the breath

hold block averaged fNIRS and fMRI data respectively for the breath hold protocol. The x-axis represents the time in seconds and the y-axis the change in HbO, HbR and HbT for the fNIRS data (Figure 4.38) and the change in BOLD signal for the fMRI data Figure 4.39.

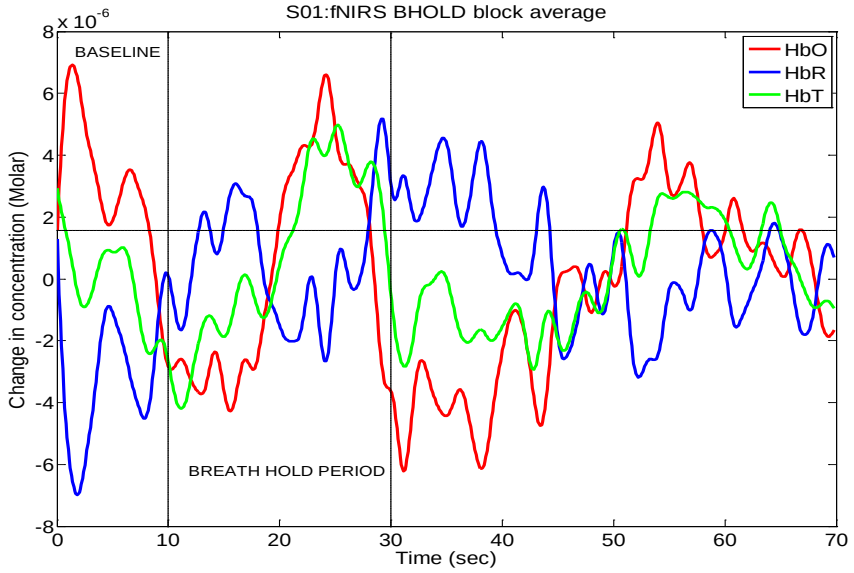

Figure 4.38: Subject 1 - fNIRS Breath Hold Block Average

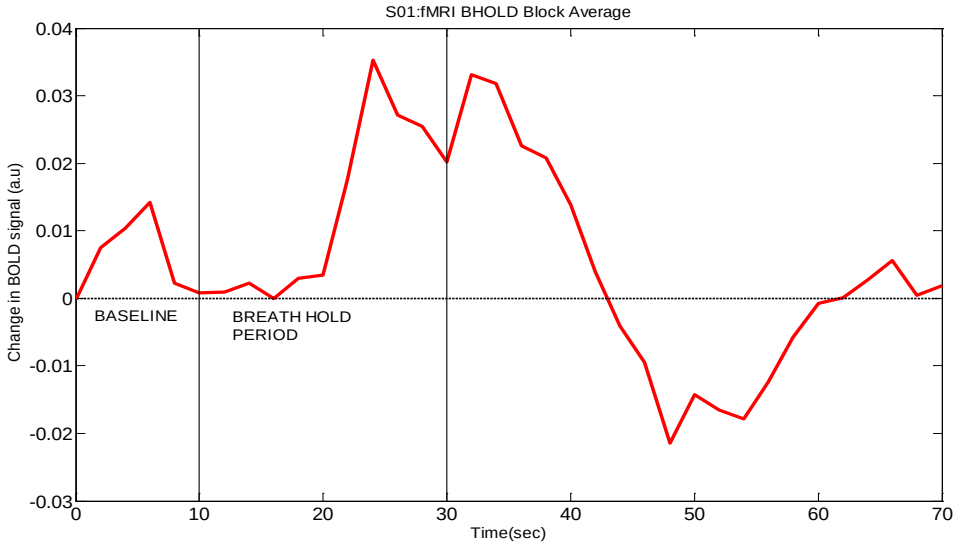

Figure 4.39: Subject 1 - fMRI Breath Hold Block Average

The block averaged breath hold data was plotted similarly for Subject 2 in Figure 4.40 and Figure 4.41 and for Subject 3 in Figure 4.42 and Figure 4.43 respectively.

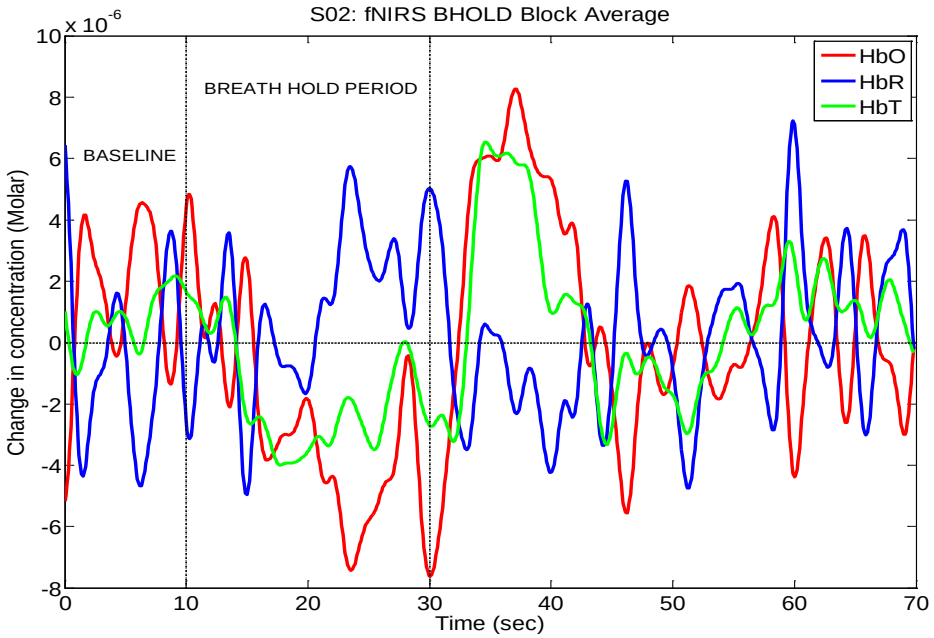

Figure 4.40: Subject 2 - fNIRS Breath Hold Block Average

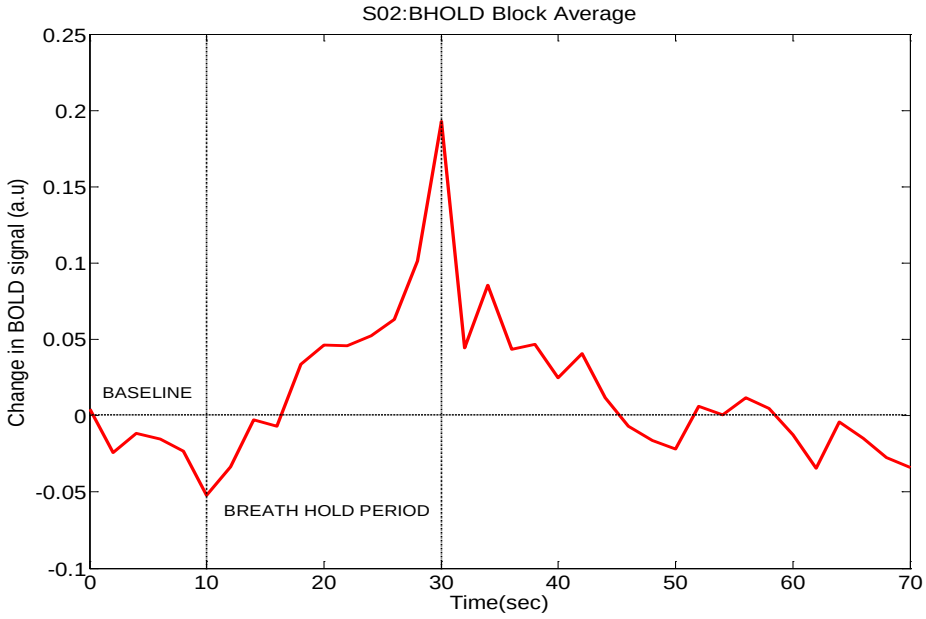

Figure 4.41: Subject 2 - fMRI Breath Hold Block Average

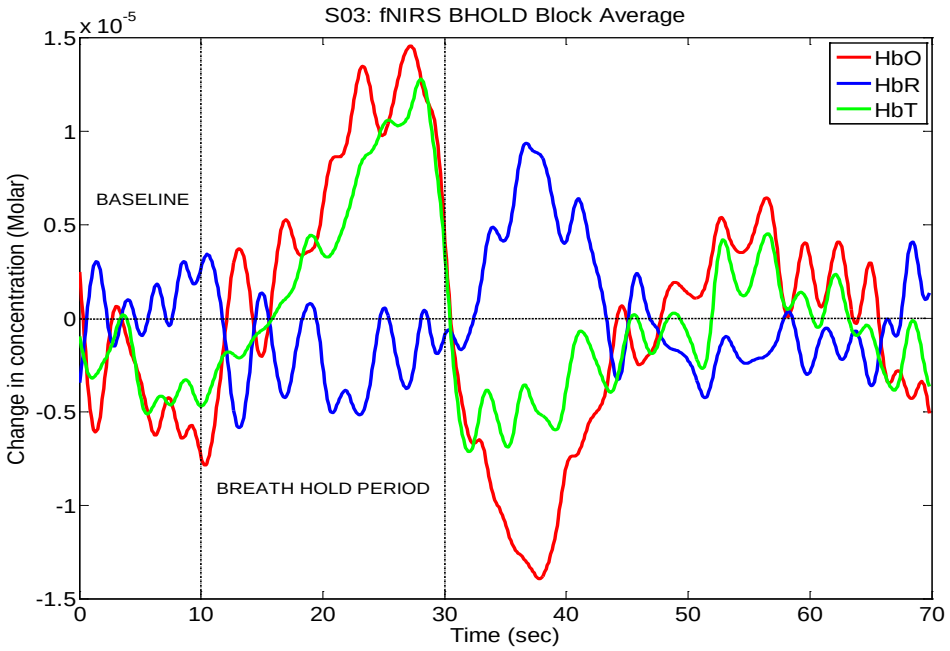

Figure 4.42: Subject 3 - fNIRS Breath Hold Block Average

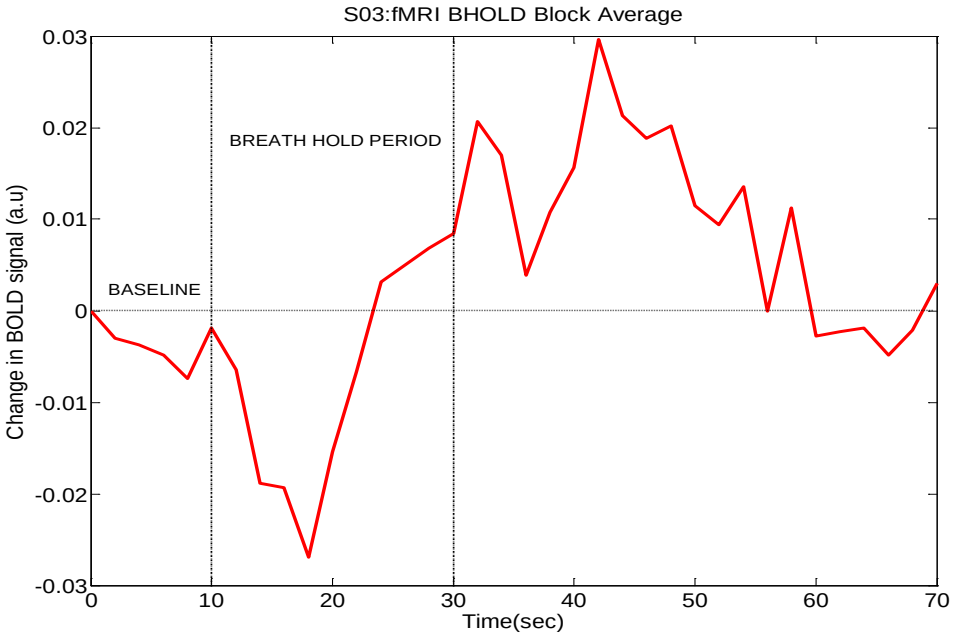

Figure 4.43: Subject 3 - fMRI Breath Hold Block Average

The next two figures, Figure 4.44 and Figure 4.45 represent the Block Averaged Breath Hold data for the average of subjects.

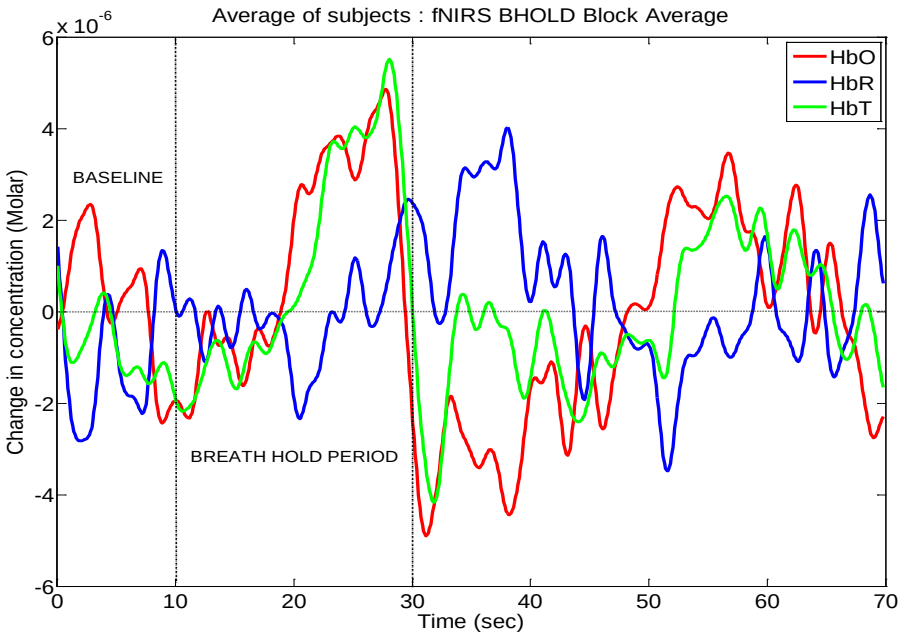

Figure 4.44: Average of subjects - fNIRS Breath Hold Block Average

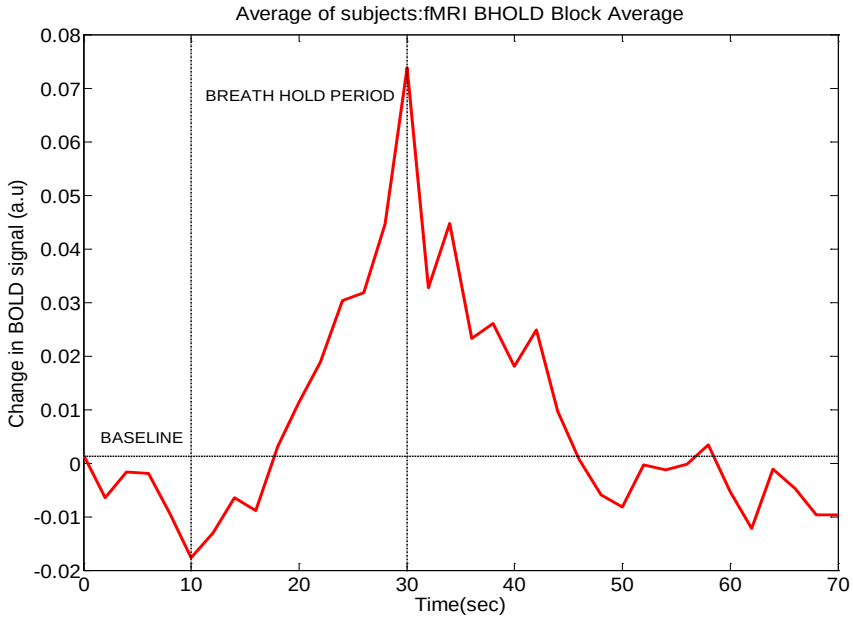

Figure 4.45: Average of subjects - fNIRS Breath Hold Block Average

4.6 Conclusions

The aim of this chapter was to compare and contrast the data that was obtained using the 2 imaging modalities. Spatial response at the highest channel of activation in fNIRS and at a similar location (location determined by vitamin E capsules), indicated that the modalities are highly spatially correlated in terms of region of activation.

Next the block averaged temporal response of the fNIRS data and the fMRI data were presented. To compare and contrast across the two imaging modalities, that data was normalized and a Pearson Correlation Coefficient 'r', was calculated of HbO with BOLD, HbR with BOLD and HbT with BOLD. Previous studies [20, 21] indicated that BOLD showed highest correlation with HbR. In this study however, BOLD showed higher correlation with HbO, than HbR and HbT in terms of the value of 'r' across the 2 s, 4 s, 8 s and the 16 s protocol. This behavior was consistent for the subjects individually and the average of the subjects.

Non-linearity in BOLD signal is a well established fact. Simultaneous fNIRS and fMRI measurements have indicated nonlinearity in HbO, HbR, HbT and BOLD signal. The nonlinear hemodynamic response behavior is very evident for Subject 1 and Subject 2 for both modalities. However for reasons not known yet, this behavior is not evident either in the fMRI data or in fNIRS data of Subject 3. Hence, this dataset was not included in the average data set for non-linear behavior. Nonlinearity is seen clearly in the averaged fNIRS and fMRI data set (for Subject 1 and Subject 2). This behavior is very important, as the data is spatially and temporally correlated and the non-linear behavior is consistent across modalities, this information is significant to analyze what BOLD signal measures exactly.

Also another important observation that has been made through this study, in that the nonlinearity in hemodynamic response behavior is only observed for smaller stimulus durations and not for longer stimulus durations. This observation is consistent in both modalities.

The algorithm that has been used in this study to model hemodynamic response is shown to work well for both the fNIRS and fMRI data. The mean square errors between the measured and the fitted data for both studies were within the 10% range. Also, most of the parameters (c2, c3 and b) that were used to model the hemodynamic response did not vary significantly. Hence, the factors that affected the time to peak, maximum amplitude and full width half maximum did not vary significantly. The reason behind the variation in parameters 'a' (that affects the initial offset in neuronal firing) and 'c1' (that affects the amplitude) is unknown as the study is in its preliminary stage; these values are more or less within range.

To summarize, a good spatio-temporal comparison has been observed between the two imaging modalities in this simultaneous study. Nonlinearity in hemodynamic response behavior exists mostly in all fNIRS and fMRI parameters. This behavior is significant though at smaller stimulus durations in both cases.

CHAPTER 5

FUTURE WORK

This study was a preliminary step in understanding how a simultaneous study could be used to correlate various parameters between two imaging modalities, to study nonlinearity in fNIRS and fMRI and to devise a method that could model the hemodynamic response based on neural adaptation theoretically modeled as a two parameter exponential equation. This study helps in understanding the correlation of BOLD with the NIRS parameters and has indicated potential application of NIRS where the temporal resolution required may be higher or MRI may not be suitable due to patient specifications(for example, patients with cerebral palsy). A few suggestions in terms of future work include:

1) The present study included the data from 3 subjects. Hence, including a larger subject pool would increase the statistical power of the study.
2) To ensure that the finger tapping task is consistent and well done across subjects, it is essential to train subjects outside the MRI Scanner so that they tap reliably. An important addition could be to include finger tapping gloves which gives us a more direct measure of the subject's performance. Using these gloves, whenever two fingers come together a circuit is completed by the glove and a trigger is sent to the recording computer.

3) Though the current fitting model fits for factors like time to peak, maximum amplitude and full width half maximum of the measured response, it does not account for the undershoot in response that occurs occasionally. It is important to identify robust fitting model that has physiological meaning and fits for the undershoot in response.
4) An alternate finger tapping protocol may be used with variable stimuli and fixed ISI respective to the stimuli duration to completely eliminate subject anticipation.
5) The results obtained in this study are significant as this is amongst very few studies that work simultaneously on fNIRS and fMRI protocols. Hence, the results should be published for reference or citations in the future.

APPENDIX A

INSTRUMENT SPECIFICATIONS

CW5 Specifications

Transmitters: Laser Sources

Number of sources.....24
Type of source.....Laser
Source wavelengths.....690 and 830 nm
Optical Output
Power per source..... 9 mW, 3 mW
Output control
Capability modulation.....On/Off, Square-wave
Connector type.....Optical SMA

Receivers: Detectors

Number of receivers..... 24
Type of receiver..... Avalanche Photo Diode
Photo sensitivity..... 0.5 A/W @ 800 nm
Gain Range..... -12 To +84 dB
Optical bandwidth..... 400-1000 nm
Signal bandwidth..... 16 kHz
Control capability..... On/Off &
programmable Gain
Connector type..... Optical SMA

External Remote Control Details:

Electrical Interface..... Serial
Control Language..... Proprietary
Data bit rate..... 5 kHz

General Physical Details (approximate as shown in photograph):

Input power.....10V AC 60 Hz @ 2.5A
Operating Temperature.....0 to 40 C
Storage Temperature.....-20 to 60 _C
Humidity..... 5 to 95 % noncondensing
Dimensions with.....Length 20 inches
Enclosure Width 20 inches
Height 17 inches
Rack Mountable 19 “width
Weight..... 100lbs in enclosure

REFERENCES

1) Theodore J. Huppert, Rick D. Hoge, Anders M. Dale, Maria A. Franceschini, David A. Boas "Quantitative spatial comparison of diffuse optical imaging with blood oxygen level-dependent and arterial spin labeling-based functional magnetic resonance imaging." Journal of Biomedical Optics 11(6), 064018 (November/December 2006).

2) A P Gibson, J C Hebden and S R Arridge, “Recent advances in diffuse optical imaging.” Phys. Med. Biol. 50 (2005) R1–R43

3) Dynot User Manual

4) www.hitachi-medical.co.jp/info/opt-e/genri-2.html.

5) Martin Schweiger, Adam Gibson, Simon Arridge, “Computational aspects of diffuse optical tomography.” 1521-9615/03 © 2003 IEEE

6) Gary Strangman, David A. Boas, Jeffrey P. Sutton,"Non-Invasive Neuroimaging Using Near-Infrared Light",Biol Psychiatry 2002;52:679–693

7) http://www.spineuniverse.com/videos/mri/

8) Kim J.G., M. Xia and H. Liu “Extinction coefficients of hemoglobin for nearinfrared spectroscopy of tissue.” IEEE Engineering in medicine and Biology Magazine March/April 2005 0739-5175/05

9) Human Physiology by Stuart Ira Fox – 9th edition August 2006

10) David A. Soltysik, Kyung K. Peck, Keith D. White, Bruce Crosson, Richard W. Briggs, “Comparison of hemodynamic response nonlinearity across primary cortical areas”, NeuroImage 22, 1117– 1127 (2004)

11) CW5 instrument user manual

12) CW5 software user manual

13) Homer user guide

14) T.J. Huppert, M.A. Franceschini, and D.A. Boas; “HomER- A graphical interface for functional NIRS analysis”.

15) ://afni.nimh.nih.gov/afni

16) ://www.pstnet.com/products/e-prime/

17) Functional Magnetic Resonance Imaging by Scott Huettel, Allen Song and
Gregory McCarthy

18) Boynton, G.M., Engel, S.A., Glover, G.H., Heeger, D.J. “Linear systems analysis of functional magnetic resonance imaging in human”, Journal of Neuroscience (V1), 16, 4207–4221 (1996).

19) Cohen, M.S., “Parametric analysis of fMRI data using linear systems methods”, NeuroImage 6, 93– 103(1997).

20) T.J. Huppert, R.D. Hoge, S.G. Diamond, M.A. Franceschini, D.A. Boas, “A temporal comparison of BOLD, ASL, and NIRS hemodynamic responses to motor stimuli in adult humans”, NeuroImage 29, 368 – 382 (2006)

21) T.J. Huppert, R.D. Hoge, A.M Dale, M.A. Franceschini, D.A. Boas, “Quantitative spatial comparison of diffuse optical imaging with blood oxygen level-dependent and arterial spin labeling-based functional magnetic resonance imaging”, Journal of Biomedical Optics (2006)

22) Andreas Kastrup, Gunnar Kruger, Gary H. Glover, and Michael E. Moseley, “Assessment of Cerebral Oxidative MetabolismWith Breath Holding and fMRI”, Magnetic Resonance in Medicine 42:608–611 (1999)

BIOGRAPHICAL INFORMATION

Renuka Parlapalli was born on September 27, 1984 in Andhra Pradesh, India. She secured her Bachelor of Engineering Honors Degree in Electronics and Instrumentation from the Birla Institute of Technology and Science, Pilani, India in July 2005. From fall 2006 she started her graduate studies in Biomedical Engineering from joint program of Biomedical Engineering at the University of Texas at Arlington and University of Texas Southwestern Medical Center at Dallas, completing it by summer 2008. She has also gained significant experience through a summer research internship position at Johns Hopkins University Her research expertise is in medical imaging, image processing and bioinstrumentation. In near future, she hopes to join a medical device industry and contribute towards cutting edge industrial projects